NASA CONTRACTOR REPORT

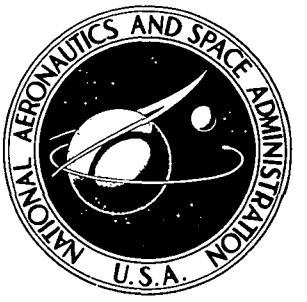

NASA CR-2371

NASA CR-2371

ANALYTICAL STUDY OF RIGIDIZED FIBROUS MATERIALS

by B. Walter Rosen, Debal Bagchi, and John J. Kibler

Prepared by
MATERIALS SCIENCES CORPORATION
Blue Bell, Pa. 19422
for Langley Research Center

NATIONAL AERONAUTICS AND SPACE ADMINISTRATION • WASHINGTON, D. C. • FEBRUARY 1974

1. Report No.	2. Government Accession No.	3. Recipient's Catalog No.
NASA CR-2371		

4. Title and Subtitle	5. Report Date
Analytical Study of Rigidized Fibrous Materials	January 1974
	6. Performing Organization Code

7. Author(s)	8. Performing Organization Report No.
B. Walter Rosen, Debal Bagchi, and John J. Kibler	TFR/7304
	10. Work Unit No.
	502-31-50-01

9. Performing Organization Name and Address	11. Contract or Grant No.
Materials Sciences Corporation Blue Bell Office Campus Blue Bell, PA 19422	NAS1-11819
	13. Type of Report and Period Covered
12. Sponsoring Agency Name and Address	Contractor Report
National Aeronautics and Space Administration Washington, DC 20546	14. Sponsoring Agency Code

15. Supplementary Notes

This is a final report.

16. Abstract

Insulation systems composed of micrometer-sized fibers bonded together with small amounts of binder have been developed for aerospace applications. The materials have a very high void content and low density and can be characterized as a rigidized network of fibers randomly oriented in three-dimensional space. In the present study, analytical models suitable for the evaluation of the mechanical behavior of rigidized fibrous materials have been developed. The models treat the material as a space frame structure and includes the effects of joint fixity and fiber curvature. The geometrical and material property variabilities are represented by a number of trusses oriented in five planes. Each truss may have different material and geometric properties. Techniques have been developed to describe the continuous material property and geometry functions as a series of descrete quantities that can be used to describe each of the trusses in the model. Parametric studies were performed to show the influence of material variables on the mechanical behavior of the material. Results of calculations show good agreement with measured properties.

17. Key Words (Suggested by Author(s))	18. Distribution Statement
Reusable Surface Insulation Rigidized Fibrous Materials Mechanical Analysis of Fibrous Materials	Unclassified-Unlimited Cat. 32

19. Security Classif. (of this report)	20. Security Classif. (of this page)	21. No. of Pages	22. Price*
Unclassified	Unclassified	79	$3.75

*For sale by the National Technical Information Service, Springfield, Virginia 22151

TABLE OF CONTENTS

ANALYTICAL STUDY OF RIGIDIZED FIBROUS MATERIALS

BY

B. Walter Rosen, Debal Bagchi
And John J. Kib ler

1. INTRODUCTION

Thermal protection during the re-entry of the space shuttle vehicle into the earth's atmosphere requires the development of an external surface insulation material having low density and moderately high temperature capability. This material must satisfy two important requirements. It must be able to provide thermal insulation and it must be strong enough to prevent failure due to thermal, mechanical, acoustric and vibratory loads. The material must also offer satisfactory resistance to damage and degradation from ground handling environments such as fuel spillage, humidity and salt spray. To satisfy these broad requirements, insulation systems have been developed having fibers bonded together with a small amount of binder material. The materials have a very high void content and a very low density. The materials may be described as rigidized fibrous materials having a random orientation of fibers in three dimensional space. Methods for analyzing such materials have not been available.

The present study involved the development of analytical material models suitable for the evaluation of the thermal and mechanical characteristics of various rigidized fibrous materials. The model treats the material as a space frame structure and includes effects due to fiber curvature and joint fixity. The present material model can be used to assess the relative effect of the material variables upon the strength under combined states of mechanical and thermal loadings. Thus, the relative merits of different materials (existing or potential) can be studied. In the present task, attention was confined to mechanical and thermal loading. The effect of acoustic, vibratory or shock loads on the structural integrity was beyond the scope of the present research activity.

2. MECHANICS OF FIBROUS MATERIALS

The literature on the mechanics of fibrous materials is limited and largely related to the mechanics of paper. The material properties of materials having a fibrous structure were treated by Cox [1]. He studied the effect of orientation of the fibers on stiffness and strength. For the planar case of fiber orientation distribution, it was shown that all possible combinations of elastic moduli may be represented by arrays of four sets of parallel fibers in appropriate ratios. Cox compared the results of the analysis with experimental results for resin bonded fibrous filled materials and reported reasonable agreement.

For materials like paper or non-woven textiles, the microscopic distribution of fibers shows an irregular geometrical pattern. Corte [2] and Dodson [3] have treated the strength and stiffness of this class of materials considering the statistical geometry of random fiber networks. The structure of this type of material is essentially two-dimensional; i.e., no fiber traverses the thickness of the sheet from top to bottom. Thus, the geometrical problem of describing the structure of this network is one in two dimensions. The basic approach to a quantitative description of a network of random lines representing the geometry of paper was outlined by Kallmes and Corte [4]. They expressed certain material characteristics in terms of measureable quantities including the fiber length, fiber width, number of fibers per unit area, eccentricity of orientation, etc. The dependent statistical measures of the material included number of fiber crossings in the sheet, mean number of fiber crossings per fiber and the mean free fiber length. These quantities influence the strength and the elastic behavior of the network.

Dodson [5] presented a statistical theory of the deformation of an inhomogeneous material under simple conditions of stress. The results of the analysis give statistical predictions of the observable dilatations and the overall modulus in terms of the statistical properties of the material. Good agreement with experimental observation is reported for porous materials in the form of flat, fibrous networks.

Rosen and Bagchi [6] studied behavior of a three dimensional fiber array by using a space frame material model. That model consists of trusses, arranged in orthogonal planes, and having elements which differ in various aspects of their geometry including fiber diameter, nodal point spacing, fiber orientation, etc. Each individual space frame element can be analyzed when subject to applied loads to determine maximum stresses in the space frame members. The failure analysis then provided a relationship between maximum allowable applied stress and the various geometric parameters of the specified element.

3. METHOD OF ANALYSIS

The Reusable Surface Insulation (RSI) materials studied are rigidized fiber networks. The analysis of RSI materials is based upon the modeling of the actual material by a space frame structure in which each section of fiber between nodes is treated as a beam having some initial curvature. The model utilizes a series

of different, regular arrays of trusses, having various orientations, to represent the actual three dimensional fiber array. This may be regarded as representing a continuous statistical distribution function by a series of discrete delta functions of differing magnitude (i.e., approximating a curve with a bar graph). Methods of translating statistical distributions of fibers into regular arrays have received some attention in the study of paper (Ref. 1 - 6). The analysis of RSI materials requires treatment of nonhomogeneous materials. When this material is subject to any loading, the average deformation of the material depends both on the physical and geometrical variabilities of its constituents. The theory of deformation of heterogeneous media in the case of multiphase bodies considering physical variability from phase to phase has been studied by a number of authors (Ref. 7 - 11). The work that is associated with the class of materials termed as paper was discussed in the previous section and is concerned basically with the effect of geometrical variability of the constituent fibers upon the elastic properties of the material.

The present work follows the concept that the three-dimensional random network of fibers can be represented by a basic set of truss elements oriented in different planes, as introduced by Rosen and Bagchi [6]. Results obtained from the analysis of that model show encouraging agreement when compared with experimental values. This has motivated the present development of a general model to evaluate the characteristic of RSI material exhibiting both geometrical and material variability. The geometrical and material variabilities of the actual material are represented by a number of trusses oriented in different planes with variable material and geometrical properties. The concept of parallel trusses is introduced to represent such geometric factors as orientation, fiber aspect ratio, eccentricity, volume fraction, etc.

Basically, the approach is to represent the continuous statistical distribution function defining fiber geometry by a series of elements having discrete values of each of the variables. This may be viewed physically as an approximate model, or it may be viewed mathematically as a discrete representation of a continuous function.

The required analysis consists of three major aspects. First, the governing equations for the material model must be defined and a method of solution established. Second, a procedure for relating the model parameters to the actual material geometry must be defined. Third, a failure criteria must be incorporated into the stress analysis procedure. Details are discussed below.

3.1 Basic Assumptions

The space model consists of an assembly of different trusses, groups of which are oriented parallel to each of five different planes (Figure 2). Any of these five planes can have any number of trusses whose interaction with one another stems from the

constraint that all have the same average strains. The analysis of this model when subject to a combined state of stress is based on the following assumptions:

1) Each of the trusses lying in any plane has the same state of average strains (which means that their edges have the same displacements).

2) The fibers within a single truss are of the same length, diameter, eccentricity and the same inclinations - oriented symmetrically with respect to X_3 axis (see Figure 1). The material variability is accounted for by having parallel trusses with different values of parameters assigned to different trusses.

3.2 Stiffness Formulation

Based on the above assumptions, the strain component in the fiber direction of any truss is given by,

$$\varepsilon^f = B.\varepsilon \tag{1}$$

where ε - material strain components;

ε^f - fiber strains;

B - transformation matrix.

Similarly, the stress in the fiber of any truss is given by,

$$\sigma^f = E.B.\varepsilon \tag{2}$$

where σ^f - fiber stresses;

E - effective fiber stiffness (including eccentricity effects).

At any stage of loading, the increase in the strain energy of each fiber link, δV, of the model due to virtual displacements, δe, can be found:

$$\delta V = f(\varepsilon, E, B, G).\delta e \tag{3}$$

where G defines fiber geometry. The total strain energy is obtained by summation over all links in a truss. Similarly, the additional external work done due to virtual displacement can be written as:

$$\delta W = \sigma.\delta e \tag{4}$$

where σ are the applied stresses.

Equating the total increase in strain energy to the additional external work to obtain the equilibrium condition, we can write

$$\sigma = C^*.\varepsilon \qquad (5)$$

where C* are the effective elastic properties of the material at any strain level. Details of the derivation are given in the Appendix A.

The above equations define the nonlinear stress-strain relations as a function of the space frame geometry and fiber stresses. A computer program has been developed and checked out to compute these stress-strain curves for a relatively arbitrary space frame geometry.

3.3 Elastic Symmetry

If the internal composition of a material possesses symmetry of any kind, then symmetry can be observed in its elastic properties. This will occur because the elastic properties are identical to the directions of symmetry which are developed in the body. The connection between symmetry of construction and elastic symmetry can be formulated in the following way: a material, in regard to its physical properties, has the same kind of symmetry as its crystallographic form. This principle can be expanded to include bodies which are not crystalline, but which possess a symmetry of structure. However, elastic symmetry is usually more extensive than geometric symmetry; in addition to the equivalent directions which coincide with the symmetric directions of the structure, other directions exist for which elastic properties are identical.

If an anisotropic body possesses an elastic symmetry, then the equations of the generalized Hooke's law are simplified. The effective elastic constants of the material model under study shows three planes of elastic symmetry. The material is orthotropic and has nine elastic constants.

3.4 Thermal Stress

For fibrous insulation materials, the principal mode of heat transfer at elevated temperature is by thermal radiation, see [13]. However, due to the random orientation of the fiber, the path of radiation will be obstructed causing a temperature gradient within the material. Since the material is under a uniform state of strain, the temperature gradient will cause thermal stresses locally within the material. These strain

components may be treated as initial strains; the stress-strain law given by equation (5) can be written as:

$$\sigma = C^* . (\varepsilon - e_T) \qquad (6)$$

3.5 Determination of the Geometry of the Truss

One of the problems of the space model is to obtain the regular geometrical orientation of truss models to represent the random oriented texture of the actual material. Corte [2] and Dodson [3], based on certain statistical data for the independent variables, provided the shape and area of the regular polygons formed by the truss members in two dimensions. In the present analysis, the model is defined by associating each fiber with one of the five reference planes. Each of these five groups of fibers is then regarded as a planar array and then statistical methods can be applied to define the geometry in each plane. As an example, the geometric variables may be regarded as independent quantities in each plane and they can be measured experimentally from enlarged photographs for that plane to determine a single variable frequency distribution function. Depending on the shape of the frequency curve, and the coefficient of variation, the area under the curve can be divided into an equal number of intervals to represent the continuous function with a fixed number of discrete variables. Detailed study of representing the random geometry with a fixed number of discrete variables is included in Appendix C.

3.6 Failure Criteria

When the model is subject to a combined state of stress, failure of the random oriented fibrous composite material may be viewed physically either as an accumulation of internal fractures caused by the breaking of fibers in any plane, or as a result of debonding of sufficient number of joints with the increase in applied stress. The class of rigidized fibrous materials dealt with here does not show any debonding effect during the experiment. As such, our main objective is to develop a failure criteria based on the fracture of individual fibers.

The statistical models proposed in the study of fracture or failure mechanics take as a starting point Griffith's theory [14] which states that the reason for the difference between the calculated strengths of materials and the actual observed values resides in the fact that there exist flaws in the body which will weaken it. This means that there will be a distribution of strengths in a given specimen in the sense that a different amount of force will be needed to fracture the specimen at one or another point. If one assumes that the flaws are distributed at random with a certain density per unit volume, the strength of a given specimen is determined by the weakest

point in the specimen. This is the basis of statistical theory of brittle fracture of fibrous materials and other solids on which much theoretical work has been done [15]. However, the problem of distribution of strength of bundles of threads (fibers) [16] cannot be treated as a problem in the distribution of smallest values because the complete bundle will not fail when its weakest member is broken.

In a real problem, the situation is probably neither that of elements in series (weakest link) nor in parallel (bundle theory), but elements distributed in rather complicated arrangement. Recently, the statistical theory of brittle fracture has been extended [17, 18] to define the failure of a fibrous body as the failure of the weakest link of a chain where each of the links represents a bundle of fibers connected in parallel.

None of these theories described above are sufficient to describe the physical phenomenon of failure of RSI material with a random oriented fibrous structure. The problem is more complicated because of the fact that the stress field is nonuniform and the distribution of fibers is random. To get an exact solution, it is necessary to derive a joint density - distribution function describing the variability of geometrical and physical parameters and then correlate the nonuniform stress field from the above distribution function with the strength distribution. First of all, it is difficult to derive a joint distribution describing all variabilities. Secondly, after the initial of crack in some region, it will be necessary to modify the distribution function at each state of loading. An exact treatment of this problem based on existing knowledge of the statistical theory of brittle fracture poses an insurmountable problem.

To simplify this problem, it is postulated in the present analysis that the material model consisting of an assemblage of truss elements is adequate to describe approximately the deformation behavior of the actual material in the pre and post crack region. With this postulation and further assumption that the truss will fail when any of its members will reach the maximum allowable stress, the probability of the failure of the complete model [19] based on the weakest element theory at a stress equal to or less than σ° is given by

$$P(\sigma^\circ) = 1 - \prod_{i=1}^{n} [1 - F(S_i)] \qquad (7)$$

Where $F(S_i)$ is the cumulative probability of failure of i th truss at a stress equal to or less than S_i and n is the total number of trusses.

Using the Weibull's distribution, the value of $F(S_i)$ is given by:

$$F(S_i) = 1 - e^{-\alpha . S_i^{\beta}} \qquad (8)$$

where the values of α and β depend on the properties of RSI material.

However, this formula is not satisfactory to describe failure conditions in the subcritical region after the initiation of a crack due to the purtubation of the stress field in the uncracked members of the trusses. To overcome this difficulty, a numerical approach is adopted based on the following definition of failure criteria to study deformation in the subcritical region. As the loading is increased on a model, at some stage, fracture is initiated in a plane by the breaking of some fibers in a particular truss. Loading will be redistributed as a result of this break into the remaining unbroken fibers in different trusses. This may lead to failure of more fibers with another redistribution of stresses. However, at some point a stable configuration may be attained, arresting the growth of damage as a result of the redistribution. During this stable condition, loading can be increased, until eventually an unstable situation will arise when any further growth of fracture will cause a complete failure of the truss model due to redistribution.

Therefore, failure of the present model can be viewed as shown in Figure (3) as a result of initiation of growth of fracture and finally due to the occurrence of an unstable situation when the reduced stiffness of the structure cannot absorb the energy released due to fracture.

It should be mentioned here that depending on the stress condition, failure of any truss may be either due to the break of any fiber under tension and compression or due to local buckling of any fiber under compression. Both modes of failure can be detected using this numerical approach.

4. PARAMETRIC EVALUATION OF ANALYSIS MODEL

Parametric analyses have been performed using the space frame analysis program to obtain a feel for the sensitivity of the results to the many input parameters. Among the variables considered are: the effect of fiber joint fixity, the effect of distribution of both fiber angle and strength on tensile strength, compressive strength, shear strength, combined shear and tension, and thermal stresses.

Figures 4 and 5 were picked at random to demonstrate the nature of the analysis. Figures 4 and 5 show the results for the RSI model with fiber edges free to rotate at the joints. Figure 4 gives the stress-strain plot of the model in some arbitrary units with one truss in each plane, while Figure 5 shows similar results for a model with five trusses in each plane, incorporating the variability of Young's modulus and ultimate stress of the fiber in the trusses within each plane.

Appendix B presents a detailed discussion of the results of the other cases considered during this study. The results clearly demonstrate that the stress geometry and fiber properties significantly effect the predicted RSI strength.

5. RSI MATERIAL EVALUATION

Before modeling RSI material as a space frame, photomicrographs of RSI were studied to determine the properties of the spatial-distribution of fibers, fiber diameter, initial curvature and fiber length to diameter ratio. Two types of RSI material were studied, the differences being primarily the diameters of the fibers. The material composed of smaller diameter fibers will hereafter be designated RSI-SDF while the material composed of larger diameter fibers will be designated RSI-LDF. Typical photomicrographs of these materials were supplied to MSC by NASA-LRC, two of which are reproduced in Figure 1. Given a least squares fit of a distribution function to the experimentally measured values, one then determined a discrete set of values to represent the continuous distribution function. Details of how the above was accomplished, along with the necessary analytical expressions are given in Appendix C. The remainder of this section will center on the results obtained from the photomicrographs of RSI and the corresponding analytical models which were developed.

The angular distribution functions used to represent the spatial distribution of fibers were

$$f(\theta) = \frac{1}{\pi} (1 + e \cos 2\theta) \tag{9}$$

and

$$f(\theta) = \frac{1 + e \cos 2 (\theta - j\bar{\theta})}{\pi + 2 e \sin 2\bar{\theta}} \tag{10}$$

Where equation (9) represents a simple elliptical distribution function and equation (10) provides symmetry in each quadrant, reflecting how one might expect a non-oriented fiber distribution to shift under processing pressures.

The coordinate axes for an RSI tile are shown in Figure 6. The fiber distribution data and least squares best fit distribution function using equation (9) are given in Figures 7 through 10. As can be seen, a considerable amount of scatter existed in the data and equation (9) does not give a wholly satisfying fit to the data for the RSI-LDF, X-Z plane (Figure 7). Note that for each group of points only one angle was measured. The spread of points about each angle was merely a convenient way of representing multiple readings.

The first set of Figures, 7 through 10, indicate that some eccentricity in the fiber distribution existed for the through-the-thickness planes, X-Z and Y-Z, for the RSI-LDF material, but that the in-plane photographs indicated a uniform, i.e., circular, distribution for both materials.

The photomicrographs of the RSI-SDF material showed mainly fiber ends present in the through-the-thickness plane. Additional photomicrographs of this material were obtained and confirm the initial photographs. Due to the lack of distinct in-plane fiber definition in the through-the-thickness planes, the fiber distribution for RSI-SDF was not obtained in these directions.

Figures 11 through 13 give the results of fitting the fiber distribution data to equation (10). The best fit to the RSI-SDF material in the X-Y plane results again in a uniform distribution, i.e., e = 0.0, and is not included with the figures. Note that the best fit curves using equation (10) appear to provide a better fit to the data than that given by equation (9). From the above data one recognizes that values of $\bar{\theta}$ can range from 0 to 25 degress along with values of e varying from 0 to over 0.2. With this information, limits can be set for the sensitivity studies such that the study results will fall in the realm of "real world" materials.

In addition to fiber orientation data, the photomicrographs were used to determine fiber diameters of the various materials. Roughly one hundred measurements were taken from photomicrographs of the various planes of material. The results of these measurements are shown in Figures 14 and 15. It is clear from these figures that the RSI-SDF material fiber diameters were essentially uniformly distributed between 1 and 3 micrometers in diameter, while the RSI-LDF material fiber diameters were roughly uniformly distributed between 2 and 6 micrometers in diameter. The RSI-LDF material, however, possessed several fibers in each plane which were up to 10-12 micrometers in diameter, which gave the photomicrograph a rather nonuniform diameter variation appearance. The RSI-SDF material, on the other hand, had little variation in diameter above 3 micrometers, giving the photomicrographs a very uniform appearance.

Fiber length to diameter measurements were virtually impossible to make from the photographs since very few fibers possessed more than one intersection point in the photomicrographs, due to masking by other fibers, and due to the fibers simply extending out of view of the photomicrograph. At the other extreme, some fibers had intersections visible every one to two fiber diameters.

5.1 RSI Model Definitions

The analytical models used to represent RSI material are described in this section. The results of fitting the experimental fiber distribution data to elliptical distributions have been used to define the range of variables to be considered,

since one cannot expect data from relatively small number of photomicrographs to completely characterize the real material. In an effort to fully cover the range and to determine the sensitivity of the results of the variables, mean fiber angles up to ± 40 degrees from vertical and eccentricities up to 0.30 have been considered.

Using the techniques described in Appendix C, the proper choices of angular positions for the fiber pairs in each plane have been made. As an example, Figures 16 and 17 give the distribution function, $f(\theta)$, and locations of fiber angles for various numbers of fibers in a plane for a mean fiber angle of zero degrees and eccentricity of zero (uniform distribution) and 0.100. The number of fibers per plane were varied to determine the number of fiber pairs required to give an adequate representation of the material. The results of this study will be discussed in the following section.

Figure 18 presents the effect of varying the preferred fiber orientation for equation (10) from zero to forty degrees. Also shown are the discrete fiber locations for each preferred orientation, assuming eight fiber pairs in a plane and an eccentricity of 0.30. While the differences in fiber position are slight, some rather pronounced effects on the strength and modulus of the material were found, as described in the following section.

Four planes were used in the models, located at positions of 0, ± 45 and 90 degrees in the 1-2 plane. The differences in results obtained from the photomicrographs did not substantiate a significant difference in distribution between the xz and yz planes, hence the fiber distributions were assumed the same in all planes.

Fiber length to diameter ratio, ℓ/d, and eccentricity, e_f, were held constant for each model, but were varied to determine the sensitivity of the results to each variable. Eccentricity was varied from zero (straight fibers) to 3.0 and ℓ/d was varied from 5 to 15. The fiber volume fraction of all models was held constant at 10%.

A fiber modulus of elasticity of 1.378×10^5 MN/m^2 (20×10^6PSI) was assumed for all cases, and for the purpose of determining geometric effects, the fibers were all assumed to have a strength of 344.5MN/m^2 (50KSI). In all cases tensile loading was applied to the 33 direction, or parallel to the planes containing the fibers.

5.2 Discussion of the Results of the Geometry Sensitivity Study

5.2.1 Number of Fiber Pairs/Plane Required

The first problem which was investigated was to determine the number of fiber pairs per plane required to give reasonable results in the space frame analysis program. Since

the cost per analysis was a strong function of the number of fiber pairs per plane, it was desirable to minimize this quantity, but not sacrifice confidence in the results. To provide an answer to this problem, a uniform distribution of fibers was assumed, with an eccentricity of 1.0. Values of ℓ/d were varied from 5 to 15 and cases were run with 5, 8 and 10 fiber pairs per plane. The results are plotted in Figure 19. As can be seen, the number of fiber pairs per plane did not affect the predicted modulus of elasticity, but did alter the strain and stress at first fiber break.

It should be pointed out that one pair of fibers at $\pm\theta$ form a truss, which is assigned to a given plane. There can be any number of trusses assigned to a plane, and five planes in the model. Thus 8 fiber pairs per plane indicates that the model had 8 trusses defined (16 fibers) in each plane.

The results appear to be fairly constant for the 8 and 10 fiber pair cases, indicating that additional fiber pairs would not significantly alter the results. It was concluded that using 8 fiber pairs per plane would give sufficient accuracy for the purpose of this study. Consequently, eight fiber pairs per plane were used in the remaining analyses. For cases where multiple ℓ/d or fiber eccentricities would be included in one model, the above conclusion would be altered since additional variables would be introduced in a single model, thus more trusses per plane could be required.

It should be emphasized at this point that the choice of a uniform fiber strength for each model resulted in the first fiber break initiating complete failureof the model. Stable configurations after the first fiber break were only obtained when fiber strengths were variable in the model. The results of the analyses have been presented as: the elastic modulus in the direction of loading, E_{33}, measured by the stress and strain at first fiber break; the ultimate tensile stress, UTS_{33}, which was simply the stress at first fiber break; and the strain at first fiber break; ε_{Y33}, which was the strain at which instability of the model was initiated.

5.2.2 Effect of Fiber Diameter

The analyses formulated for the space frame analysis program indicate that, at least for zero fiber curvature, the results are independent of fiber diameter and are a function of the fiber length to diameter ratio. In addition, since the model

was based on the analysis of a representative unit volume, when one specified fiber angle and length to diameter ratio, the program calculates the appropriate fiber diameter for each fiber, consistent with the dimensions of the unit volume. It is possible to generate a model having the same fiber diameters and ℓ/d for all fibers by specifying the length of truss for each fiber pair, provided the lengths remain within the unit volume.

As a check on the program and to determine if different fiber diameters affected the results, cases were run of the same model with constant fiber diameters of 5 micrometers, 0.318 mm, and variable fiber diameters. A fiber distribution with $\theta=0$ and eccentricity equal to 0.2, and fiber eccentricity (curvature defined by initial displacement at the center of each fiber in terms of fiber diameters) equal to 1.00, keeping the results consistent for a fiber volume fraction of 0.10. The results are plotted in Figure 20. As can be seen, the results are indeed independent of fiber diameter and the length to diameter ratio is the primary variable.

5.2.3 Effects of Fiber Distribution Eccentricity

With the above preliminary considerations satisfied, the more important effects of the distribution of fibers in the material were considered. The effects of eccentricity of fiber distribution, orientation of the fiber distribution, eccentricity of the individual fibers and fiber length to diameter ratio were investigated.

First, the eccentricity of the fiber distribution was varied, keeping the mean angle equal to zero and the eccentricity of the individual fibers equal to 1.0. The results are plotted in Figures 21 and 22 for various values of ℓ/d. Note that eccentricity of the fiber distribution has virtually no effect on the strain at first fiber break although modulus of elasticity and applied stress at first fiber break increase significantly with increased distribution eccentricity. The results also show a consistent, although not large, effect of fiber length to diameter ratio. One would initially expect lower values of ℓ/d to yield higher strengths since the truss members are becoming shorter for a given diameter, and the results indicate the opposite effect, Figure 22. However, the fiber eccentricity was held constant for these cases, which means that all center span initial deflections were one fiber diameter. This implies that for the smaller ℓ/d values the fibers had much higher initial curvature than for the higher ℓ/d values, and the higher initial curvature resulted in decreased strength, hence, the results are consistent.

5.2.4 Effects of Orientation of Fiber Distribution On Properties

The effects of the orientation of the fiber distribution defined by equation (10) on modulus of elasticity, strength, and strain at first fiber break are shown in Figures 23 through 25, respectively for various values of eccentricity of the fiber distribution, holding ℓ/d equal to 10 and eccentricity of the individual fiber equal to 1.0.

Note that as the eccentricity of the distribution increases, the effect of orientation of the distribution becomes significant on the resulting strength and modulus of elasticity. As much as a 20% change in modulus and strength occurs for an eccentricity of 0.3, varing orientation from 0 to 40 degrees. Note, however, that the orientation of the fiber distribution has essentially no effect on strain to first fiber break, Figure 25, regardless of the value of the eccentricity of the distribution (i.e., a maximum strain change of only 0.6% for an eccentricity of 0.3).

Also plotted on Figures 23 and 24 are the distribution eccentricities and orientations obtained from fitting equation (10) to the photomicrograph data. For the basic fiber properties assumed, i.e., $\ell/d = 10$, fiber eccentricity = 1.0, fiber modulus = 1.378×10^5 MN/m^2 (20×10^6PSI), fiber strength = 344.5 MN/m^2 (50KSI), the figures indicate that the RSI material should have a modulus of elasticity between 1350 and 1450 MN/m^2, and a strength between 2.5 and 2.7 MN/m^2, and a strain at the onset of instability of roughly 0.178%. Naturally, other assumptions regarding fiber modulus and strength would alter these results. A change in fiber ℓ/d value will alter the result a small amount, similar to the changes seen in Figures 21 and 22, but a change in fiber eccentricity would greatly alter the results as discussed in the following section.

5.2.5 Effect of Fiber Eccentricity

Initial fiber curvature affects were examined by considering fiber distributions with $\bar{\theta} = 0$, distribution eccentricities of 0.0 and 0.3, and fiber length to diameter ratios of 10 and 15. The initial fiber curvature, fiber eccentricity, was varied from 0.0 to 3.0. The results are shown in Figures 26 through 28.

As can be seen in Figures 26 through 28, the fiber eccentricity produces the greatest overall effect on the strength characteristics of the material. The results show that decreasing the fiber eccentricity from 1.0 to near 0, one can obtain an increase in elastic modulus of 160%, a corresponding increase in strength of near 280%, along with 40% increase in strain to failure. Increasing the initial fiber eccentricity over 1.0 results in decreases in modulus of elasticity and ultimate strength, but increases in strain to failure. The significant result here is shown in Figure 28, in that the strain at first fiber break goes through a minimum value at slightly over an initial eccentricity of 0.50.

A minimum strain value for a given fiber eccentricity indicates that if one desires to increase the strength of the material, processing which does not impart initial curvature of the fiber between intersections will produce the best results. Very small initial curvature will have a large effect on all properties. Large values of initial curvature will result in increasing strain to failure, but at the expense of both strength and modulus. Since a change in modulus will result in changing the thermal strains induced in the material, a trade-off study

of thermal strain versus modulus and potential strain to failure versus modulus is required to determine the potential benefit of trying to alter the initial fiber curvature.

6. DISCUSSION

The previous sections have described the method of analysis and various parametric evaluations of RSI material which have been performed. The merit of the analytical model is apparent in that one can obtain, at a minimum, some "feel" for the type and magnitude of change in properties which one might expect from control of the various parameters during material manufacture. Thus, the analytical studies may be used as a basis for determining the desired microstructural changes in RSI material to improve the mechanical properties of the material.

Further confidence in the ability of the analytical model to predict RSI material properties can be obtained from comparison of the predicted properties with those measured and reported on the material. A direct comparison is not easy however, since the fiber length to diameter ratio and initial curvature could not be easily defined from the photomicrographs. Consequently, a complete geometrical description of the material is not available. In addition, the measured strength parameters exhibit considerable variations, further complicating a direct comparison between measured and predicted properties. It would appear that a reasonable comparison can be obtained if for the experimental range in modulus of elasticity, one chooses a range in model parameter (fiber eccentricity for example) to correspond to the same range of predicted modulus. Then, using the same model geometry ranges compare the expected range of ultimate tensile strength and strain to failure with the experimentally observed ranges.

The above described approach has been used to generate Figure 29. The mechanical properties were those reported for the RSI-LDF. As can be seen, a value of fiber eccentricity ranging from 2.2 to 3.2 produces predicted elastic moduli in the measured range. Using the same range for fiber eccentricity, the analytical model slightly over predicts the stress at failure but gives a reasonable estimate of the strain to failure. The analytical model is thus capable of predicting realistic mechanical properties for the RSI material. Verification of the changes in properties with changes in microstructure will naturally require extensive test data on samples with known microstructure.

The results of the RSI material model studies indicate that small diameter fibers can provide equivalent structural capability to large diameter fiber structures, provided that the joint spacings are comparable. Structural properties have been shown to be a strong function of the orientation and eccentricity of the fiber distribution function, which indicates one possible means of tailoring material properties. In addition, initial fiber curvature has been shown to be a significant variable affecting properties, and hence, may provide a means of increasing strain to failure of future materials.

7. CONCLUSIONS AND RECOMMENDATIONS

A suitable micromechanics model has been developed to assess the strength characteristics of rigidized fibrous material having a random oriented geometry in three dimensions. The basic assumptions and the method of analysis are reported in section three of the present report. The merit of the model lies in its ability to deal with any arbitrary geometrical configurations and also any combination of mechanical and thermal loadings. The model can also deal with the spatial variability of other parameters, like fiber eccentricity, length to diameter ratio, Young's modulus, strength of the fiber, etc. Results have been obtained for a large number of cases under different combinations of thermal and mechanical loadings. Some of these results when compared with experimental results obtained previously [6] for RSI material showed good agreement.

It is naturally desirable to have more information on the experimental work done on different low density materials under different loading conditions. Comparison of these experimental works with the present analytical results will give a better understanding of the accuracy and reliability of the present model. In this respect, we can say that based on the results obtained, a qualitative assessment of the merit of the present model has already been established.

The analytical model for RSI material has demonstrated sufficient accuracy in predicting properties. Consequently, future analytical studies should be based on exercising the present model with the aim of determining the material properties such as fiber distribution, eccentricity and orientation, initial fiber curvature and material density which would be required to meet given sets of strength goals. Studies of this type should include goals such as combined loading strengths and combined mechanical and thermal stress capability. Thus, the analytical model can help guide future material development.

Most of the results presented here have considered different cases of static loads and thermal loads. However, structural material is often subject to acoustic, vibratory or shock loads. Therefore, a study of their effects should be considered as a part of the future recommendation for research activity.

REFERENCES

1. Cox, H.L., "The Elasticity And Strength Of Paper And Other Fibrous Materials", British Journal of Applied Physics, Vol. 3, March 1952.

2. Corte, H., "Statistical Geometry of Random Fiber Networks", Conference on Structure, Solid Mechanics and Engineering Design in C. E. Structures, Southampton, 1969.

3. Dodson, C.T.J., "The Failure Of Bonds During The Fracture Of A Random Fibrous Network", Solid Mechanics and Engineering Design in C. E. Structures, Southampton, 1969.

4. Kallmes, O. and Corte, H., The Structure Of Paper: I. The Statistical Geometry Of An Ideal Two Dimensional Fiber Network, Tappi, 43,737-752, 1960.

5. Dodson, C.T.J., "Some Statistical Considerations In The Analysis Of The Deformation Of Inhomogeneous Materials", Solid Mechanics and Engineering Design in C.E. Structures, Southampton, 1969.

6. Rosen, B.W. and Bagchi, D.K., "Material Model Studies", in NASA CR-112038 (R.A. Tanzilli, editor).

7. Paul, B., "Prediction Of Elastic Constants Of Multiphase Materials", Trans. AIME, 218, 36, 1960.

8. Budiansky, B., "On The Elastic Moduli Of Some Heterogeneous Materials", J. Mech. Phys. Solids, 13, 223, 1965.

9. Hashin, Z. and Rosen, B.W., "The Elastic Moduli Of Fiber Reinforced Materials", J. Appl. Mech., 31, 223, 1964.

10. Beran, M.J., "Statistical Theory Of Heterogeneous Media", Int. Conf. on the Mechanics of Composite Materials, May 8, 9, 10, 1967, Philadelphia.

11. Hashin, Z., "Theory Of Fiber Reinforced Materials", NASA Contract No. NASA-CR-1974.

12. Lekhnitskii, S.G., "Theory Of Elasticity Of An Anisotropic Body", Holden-Day, Inc.

13. NASA Contract Report No. NASA CR-112038, April 1972.

14. Griffith, A.A., "The Theory Of Rupture", Proc. Int. Cong. App. Mech., Delft 1, 55, 1924.

15. Epstein, B., "Statistical Aspects Of Fracture Problems", J. App. Phys., Vol. 19, 1948.

16. Daniels, H.E., "The Statistical Theory Of The Strength Of Bundles Of Threads I", Proc. Roy. Soc. (London) 183, 405, 1945.

17. Gucer, D.E. and Gurland, J., "Comparison Of The Statistics Of Two Fracture Modes", J. Mech. Phys. Solids, 10, 365, 1962.

18. Rosen, B.W., "Tensile Failure Of Fibrous Composites", AIAA Journal, 2, 1985, 1964.

19. Bolotin, V.V., "Statistical Methods In Structural Mechanics", Holden-Day, Inc.

SYMBOLS LIST

A - Cross sectional area of fiber

a,b, c- Cell edge dimensions

B - Transformation Matrix

C* - Composite Stiffness Matrix

d - Fiber diameter

e - Strain components

E - Axial fiber modulus

E' - Effective fiber modulus

ℓ - Fiber length between intersections

L - Total fiber length in cell

n - Number of bays in cell

v - Cell volume

B_i - Orientation of fiber in given plane

δ - Initial midspan fiber deflection

δe - Variation in cell strain

ΔE - Increase in cell strain energy

ϕ_i - Orientation of vertical plane in cell

σ_{ij} - Stress components

APPENDIX A - GOVERNING EQUATIONS

A. Derivation of Stress/Strain Relation:

The basic assumptions underlying the derivation of stress/strain relation of the space frame model have been discussed in Section 2. With these assumptions, the strain component in the fiber direction of any truss is given by

$$e^f = B.e \tag{A-1}$$

where

$$B^T = \begin{matrix} \cos^2\phi_i \cdot \cos^2\beta_{ij} \\ \cos^2\beta_{ij} \cdot \sin^2\phi_1 \\ \sin^2\beta_{ij} \\ -\sin 2\phi_i \cdot \cos^2\beta_{ij} \\ -\sin\phi_i \cdot \sin 2\beta_{ij} \\ -\cos\phi_i \cdot \sin 2\beta_{ij} \end{matrix} \quad ; \; e = \begin{matrix} e_{11} \\ e_{22} \\ e_{33} \\ e_{12} \\ e_{23} \\ e_{13} \end{matrix}$$

ϕ_i is the angle of orientation of the truss with reference to the x axis, and β_{ij} is the angle of orientation of the fiber in any truss with the angle of orientation ϕ_i with reference to the x axis. Similarly, the stress in the fiber of any truss is given by

$$\sigma^f = E'_{ij} \; B \; e \tag{A-2}$$

where in the case of tension in the fiber

$$E'_{ij} = \frac{E\,(1+\alpha_{ij})^2}{4(2+3\alpha_{ij})(a_{ij})^2 + (1+\alpha_{ij})^2}$$

$$\alpha_{ij} = \frac{16\sigma_f}{\pi^2 E_{ij}} \left(\frac{\ell}{d}\right)^2_{ij}$$

$$\ell_{ij} = \frac{1}{2}\frac{L_{ij}}{n_{ij}} \cdot \sec\beta_{ij}$$

and in the case of compression in the fiber

$$E'_{ij} = \frac{E_y(1-\alpha_{ij})^2}{4(2-\alpha_{ij})(a_{ij})^2 + (1-\alpha_{ij})^2}$$

$$\alpha_{ij} = \frac{16\sigma_f}{\pi^2 E_{ij}} \left(\frac{\ell}{d}\right)^2_{ij}$$

$$\ell_{ij} = \frac{1}{2}\frac{L_{ij}}{n_{ij}} \sec\beta_{ij}$$

At any stage of loading, the increase in strain energy of the model due to virtual displacement is given by

$$\Delta E = Ve^T \left[\sum_{i=1}^{5} \sum_{j=1}^{4} D_{ij} \, \ell_{ij} \, A_{ij} \right] \qquad \text{(A-3)}$$

where $Dij = \Sigma B^T.E_{ij}.B$ and the summation is carried out over all free lines in a truss. Similarly, the additional external work done due to virtual displacement can be written as

$$AW = V. \sigma. \delta e^* \qquad \text{(A-4)}$$

where

$$\sigma = [\sigma_{11} \quad \sigma_{22} \quad \sigma_{33} \quad \sigma_{12} \quad \sigma_{23} \quad \sigma_{13}]$$

Equating the total increase in strain energy to the additional external work for the equilibrium condition, we can write

$$\sigma = C^*.e; \qquad \text{(A-5)}$$

or $\sigma_{ij} = C^*_{ijkl} \cdot e_{kl}$

where, $C^*_{ijkl} = \frac{1}{V} \sum_{i=1}^{5} \sum_{j=1}^{4} D_{ij} \cdot \ell_{ij} \cdot A_{ij}$

A.2 Modification of Stiffness for Clamped Ends

The effective value of Young's modulus used in the equation (A-2) represents the nonlinear axial stiffness for fiber links with simply supported ends. The necessary modification for the clamped ends can be incorporated by applying moments of both ends such that the end slope becomes zero under axial compression or tension. In that case, the expressions (A-2) for the nonlinear axial stiffness for any member are given by

$$E'_{ij} = \frac{\alpha E}{\alpha + 4 \left[2e \, \delta/d + (\delta/d)^2 \right]} \qquad \text{(A-6)}$$

where $e = a/\alpha$

$$\delta/d = \frac{e\alpha}{1-\alpha} \left(1 - \frac{\pi}{2} \frac{1-\cos u}{u \sin u} \right)$$

$$u = \frac{\pi}{2} \sqrt{\alpha}$$

for the case of compression, and by

$$E'_{ij} = \frac{\alpha E}{\alpha+4\ [2e(\delta/d) + (\delta/d)^2]}$$

$$e = a/d$$

$$\delta/d = \frac{e\alpha}{1+\alpha}\ [1 - \frac{\pi}{2u\coth\frac{u}{2}}]$$

$$u = \frac{\pi}{2}\ \sqrt{\alpha}$$

for the case of tension.

To prevent an unstable kinematic condition due to the relative rotation of bars of joints, the model must have at least one truss in the horizontal plane.

APPENDIX B - RSI MODEL EVALUATIONS

The basic formulation, failure criteria and the method of analysis for the RSI model have been discussed in Section 3. The present section will deal with results obtained using the material model to study the effect of geometric and material variability on the strength of rigidized fibrous material undedifferent loading conditions. The model essentially consists of a set of parallel trusses placed in five different planes as discussed in Section 3. The analysis was done initially considering that the fiber between any two joints was free to rotate at the edge. However, subsequently the analysis has been modified to incorporate the reality that the fiber is clamped against rotation at both ends. Details of the results covering the strength of the model under tension, compression, shear and combined loadings are discussed below.

B.1 Comparison Between the Free and Clamped Edge:

In Figure B-1a, a comparison is drawn between the results obtained for the free edge case and the clamped edge case. The model considered consists of six trusses in each plane and is subject to pure tension in the vertical direction. Angle of orientation of the fibers and the variation of strength from truss to truss in any plane are shown in Figures B-1b and B-1c, respectively. As shown in Figure B-1a, there is a considerable difference in results between free edge and clamped edge, and therefore, justifies the modification to incorporate an

approximation to joint fixity. Results in Figure B-1a also show a progressive failure as discussed under failure criteria in the previous section.

B.2 Tension

B.2.1 Study of the Distribution of Angle of Orientation:

Figures B-2 - B-6 refer to the different plots of the same model having six trusses in each of the five planes. The material and geometrical properties of the model are shown in Figure B-2. The model is subject to a uniform tension in the vertical direction and the ultimate strength of the model is determined for a constant volume fraction of 0.167 percent for each truss with the different distribution of the angle of orientation as shown in Figures B-5a to B-5h. The results obtained are shown in Table B-I. It is clearly observed that the different orientation has a significant influence on the ultimate strength of the model. Stress/strain plots shown in Figures B-2 to B-4 refer to the distribution of the angle of orientation of the fiber as shown in Figures B-5a, b, and c, respectively. Curves marked (1) show the results obtained using variable volume content for different trusses as shown in Figure B-6, and curves marked (2) refer to the case when the volume content is constant.

B.2.2 Study of the Effect of the Strength Distribution:

Table B-II presents the results of the same model with the angle of orientation of the fiber given by Figure B-5b to study the effect of different strength distribution as shown in Figures B-7a to B-7e. Cases 2, 3 and 4 exhibited the progressive type of failure postulated by the authors in a previous section. Table B-II clearly shows that the distribution of strength of the fiber can have a considerable effect on the ultimate strength of the RSI model.

B.3 Compression

B.3.1 Study of the Distribution of Angle of Orientation:

Details of the space frame model for the study of the compressive strength of RSI material are shown in Figure B-8. It consists of four vertical planes oriented at angles of 0, +45, -45, 90 and one horizontal plane. Each of the vertical planes has six trusses with all parameters constant except the angle of orientation of the fibers. The values of the constant parameters are also shown in Figure B-8. The model is subject to uniform compressive load in the vertical direction and the failure load is obtained for a constant volume content of the fibers equal to 5% with the different distribution of the angle of orientation as shown in Figures B-5a to B-5h. The

results are given in Table B-III. These results when compared with the ultimate loads obtained for the case of tension are presented in Table B-I show a little difference in failure loads. This difference may, however, be significant at higher aspect ratios between fiber joints. One important thing to be noticed when comparing the results is that the effect of the distribution type of the angle of orientation of the fibers on failure loads is similar.

B.3.2 Study of the Effect of the Strength Distribution:

To observe how the variability of the strength distribution affects the failure strength of RSI model, the example under Case (b) in Table B-III with the distribution type of the angle of orientation given in Figure B-5b were studied using different strength distributions as shown in Figures B-7a to B-7e. In all cases, trusses with similar fiber orientation in each plane have the same strength. Results obtained are tabulated in Table B-IV. It is clearly observed from Table B-IV that the distribution of strength has a significant effect on the ultimate strengths of the model, the nature of effect being the same as in the case of tension. Cases 2, 3 and 4 of Table B-IV exhibited the progressive type of failure as postulated by the authors under the combined effect of variability of the angle of orientation and strength distribution.

B.4 Shear

B.4.1 Study of the Distribution of Angle of Orientation:

The parametric details of the space frame model used for the study of the shear strength of RSI material are shown in Figure B-8. It is the same model that is used for the study of failure loads under tension and compression. The model is subject to pure shear load in the 1-3 plane and the failure load is obtained for a constant volume content of the fibers equal to 5% with the different distribution of the angle of orientation as shown in Figures B-5a to B-5h. Results obtained are given in Table B-V. These results when compared with the corresponding values obtained under pure tension show a marked difference. Whereas in the cases (a), (c) to (f) and (h), failure loads obtained are lower, cases (b) and (g) show higher values for ultimate loads. The reason may be attributed to the different nature of effect of distribution angle on the ultimate strength of the material.

B.4.2 Study of the Effect of Strength Distribution:

In the examples discussed above, strength of the fiber is assumed constant from truss to truss. However, in actual material, a sample of fibers shows a marked difference in their strength from fiber to fiber. To study this effect on the ultimate strength of the model, Case (b) in Table B-V is subject to different kinds of strength distribution as shown in Figures B-7a to B-7e, keeping the angle of orientation of the fibers the same. It should be noted that trusses in different planes with the same angle of orientation have the same strength values; results are given in Table B-VI. Also shown are the results obtained by reversing the order of maximum allowable stresses in the trusses in each plane. That is, since the initial model assigned a specific fiber strength to each fiber, a different material model can

be generated by simply reversing the strength assignments. The result could be, for example, an initial case where the strongest fibers are oriented towards the applied load direction and a subsequent case where by simply changing strength assignments, the weakest fiber could be oriented towards the loading direction. It should be observed that changing the order of maximum allowable stresses from truss to truss, results for the ultimate stress of the RSI material can be significantly different. Because of these differences, one should model strength variability by creating N parallel trusses where each truss has its own strength. Thus, if M fiber angles are defined, one would create a model with N * M fiber pairs per plane.

B.5 Combined Shear and Tension

B.5.1 Study of the Distribution of Angle of Orientation:

Details of the space frame model for the study of the strength of RSI material under combined tension and shear are shown in Figure B-8. It consists of four vertical planes oriented at angles of 0, +45, -45, 90 and one horizontal plane. Each of the vertical planes has six trusses with all parameters constant except the angle of orientation of the fibers. The values of the constant parameters are also shown in Figure B-8. The model is subject to combined uniform tension and shear in the vertical direction and the failure load is obtained for a constant volume content of the fibers equal to 5% with the different distribution of the angle of orientation as shown in Figures B-5a to B-5h. The results are given in Table B-VII . These results, when compared with the results obtained for the case of tension only and shown in Table B-I, show a significant drop in the ultimate stress due to the presence of shear. A similar comparison results when Table B-VII is compared with results obtained for the case of shear and shown in Table B-VI.

B.5.2 Study of the Effect of Strength Distribution:

In the examples discussed above, strength of the fiber is assumed constant from truss to truss. However, in actual material, a sample of fibers shows a marked difference in their strength from fiber to fiber. To study this effect on the ultimate strength of the model, Case (b) in Table B-VII is subject to different kinds of strength distribution as shown in Figures B-7a to B-7e, keeping the angle of orientation of the fibers the same. It should be noted that trusses in different planes with the same angle of orientation have the same strength value. Results are given in Table B-VIII. Results clearly show that using the variable strength distribution, the ultimate stress of the material can be significantly reduced.

APPENDIX C - RSI MATERIAL REPRESENTATION

C.1 Discrete Representation of a Continuous Distribution Function:

The space frame analysis program requires representing continuous distribution functions with a discrete number of points. Spatial orientation of fibers, fiber diameters, length between

fiber intersections, fiber eccentricities and fiber strengths all possess continuous distribution functions. Analytical representation of RSI material requires identifying a deterministic set of fiber properties which can be modeled with a finite number of trusses with fixed properties. The following section describes how a continuous distribution can be represented by a discrete distribution of finite number of samples. In particular, the spatial distribution of fibers in any given plane is considered. However, once the continuous distribution function for any of the variables is defined, the discrete representation of the variable can be determined in an analogous fashion.

It is first assumed that the continuous distribution function of a variable is known, in this case the angular orientation of RSI fiber in a given plane. It has been assumed that the distribution can be represented as a first approximation by an elliptical distribution $f(\theta)$ such that

$$f(\theta) = \frac{1}{\pi} (1+e \cos 2\theta) \qquad \text{(C-1)}$$

where e is a measure of the eccentricity of the ellipse and θ is understood to be the angle of a fiber as measured from the mean angle or preferred fiber orientation. In practice the mean angle, $\bar{\theta}$, and eccentricity can be determined by using scanning lines, on photomicrographs of RSI material. Namely, the number of fiber intersections with the scanning line, versus orientation of the scanning line will provide an experimental distribution of $f(\theta)$. A large number of scanning lines located at various areas of RSI material will be employed to give a good representation of $f(\theta)$. From the experimental representation of $f(\theta)$, the mean value of θ can be found and the eccentricity can be determined in a least squares sense, the results of which are described in the following section.

The discrete representation of $f(\theta)$ is given by

$$g(\phi) = \sum_{-N/2}^{N/2} \frac{1}{N} \phi_i \qquad \text{(C-2)}$$

where N is the total number of points and $\phi_{-i} = -\phi_i$ implying that ϕ_i is normalized with respect to the mean such that the mean values of $f(\theta)$ and $g(\phi)$ are zero. Specific values of ϕ_i are determined as follows:

$f(\theta)$ is divided into N regions such that

$$\int_{\theta_{n-1}}^{\theta_n} f(\theta)\, d\theta = \frac{1}{N} ; \quad n = 0, 1, \ldots, N \qquad \text{(C-3)}$$

and one value of ϕ_i is located within each resulting interval. Each ϕ_i could be placed anywhere within the interval θ_{n-1} to θ_n, and the general solution requires satisfying the first N+1 moments of $f(\theta)$ in order to determine each ϕ_i location. However, a reasonable approximation of $f(\theta)$ can be made by placing all values of ϕ_i in the same relative position within θ_{n-1} and θ_n and minimizing the difference between the second moments of $f(\theta)$ and $g(\phi)$. One thus obtains the following expression to be solved for α, the position of the discrete variable ϕ_i between θ_{n-1} and θ_n

$$\sum_{1}^{N/2} \frac{2}{N} \{\theta_{N-1} + \alpha (\theta_n - \theta_{n-1}) \}^2 - S = 0 \qquad \text{(C-4)}$$

where $S = \frac{1}{2} (\frac{\pi^2}{6} - e)$ is the variance of $f(\theta)$

$\theta_{n-1} \rightarrow \theta_n$ defines the equal area intervals of $f(\theta)$

N is the number of fibers = $\frac{1}{2}$ the number of discrete trusses (each truss has $\pm\theta$ fibers)

An example is tabulated in Table C-1 giving the desired positions of ϕ_i for various values of N. A graphical representation of two continuous distributions for e=0.3 and 0.95 along with the discrete representations of the distributions are given in Figures C-1 and C-2.

The above approach is valid for a standard elliptical distribution. However, when one considers how a preferred mean value of fiber orientation may occur during manufacture, a slight modification to the elliptical distribution appears appropriate. Assuming that the manufacturing process starts with a slurry of completely randomly oriented fibers, and then pressure is applied to compress the slurry, it is reasonable to assume that the fiber distribution will be symmetric about both the in-plane and through-the-thickness directions. This can be accomplished by defining $f(\theta)$ such that

$$f(\theta) = \text{const.} \; (1 + e \cos 2(\theta - j\bar{\theta})) \qquad \text{(C-5)}$$

where

$j = 1$ if $0 \leq \theta \leq \pi/2$

$\pi < \theta \leq 3\pi/2$

$j = -1$ if $\pi/2 < \theta \leq \pi$

$3\pi/2 < \theta < 2\pi$

and results in the distribution shown in Figure C-3. The function, $f(\theta)$, must be normalized such that

$$\int_0^{\pi} f(\theta)\, d\theta = 1.0 \qquad \text{(C-6)}$$

which results in

$$f(\theta) = \frac{1 + e \cos 2(\theta - j\theta)}{\pi + 2e \sin 2\bar{\theta}} \qquad \text{(C-7)}$$

Note that, when normalized, the constant for $f(\theta)$ becomes a function of the orientation and eccentricity of the distributor. Although the process is slightly more involved algebraically, equal area intervals and discrete locations for placement of discrete points can be determined in the same manner as previously outlined. In addition, data points taken from RSI photomicrographs can be fit to equation C-7 in the least squares sense to define $\bar{\theta}$ and e; the solution involving solution of a pair of non-linear equations to determine $\bar{\theta}$ and e.

C.2 Least Squares Curve Fit to Distribution Functions

Given data from the photomicrographs of RSI material which can be tabulated as number of fiber intersections, f_i, with scanning line versus angular orientation, θ_i, of scanning line, one can determine the best fit values of e and $\bar{\theta}$ in the following manner.

Define the sum of the squared residuals as

$$V = \sum_1^N \left\{ f_i - \frac{1 + e \cos 2(\theta - \bar{\theta})}{\pi + 2e \sin 2\bar{\theta}} \right\}^2 \qquad \text{(C-8)}$$

Since it is desired to minimize V by proper selection of e and $\bar{\theta}$, we require

$$\frac{\partial V}{\partial e} = 0 \qquad \text{(C-9)}$$

$$\frac{\partial V}{\partial \bar{\theta}} = 0$$

Taking the partial derivatives, and after some manipulation, one can solve each equation explicitly for e in terms of $\bar{\theta}$. as shown below:

From $\frac{\partial V}{\partial e} = 0$ one obtains

$$e = \frac{A_2 \cos 2\bar{\theta} - A_1 \sin 2\bar{\theta}}{A_3 \sin^2 2\bar{\theta} + A_4 \cos^2 2\bar{\theta} + A_5 \sin 2\bar{\theta} \cos 2\bar{\theta}} \qquad \text{(C-10)}$$

where

$$A_1 = 2\pi \Sigma f_i - 2N - \pi \Sigma (\pi f_i - 1) \sin 2\theta_i$$

$$A_2 = - \pi \Sigma (\pi f_i - 1) \cos 2\theta_i$$

$$A_3 = 4 \Sigma f_i + \pi \cdot \Sigma \sin^2 2\theta_i - 2\Sigma (\pi f_i + 1) \sin 2\theta_i$$

$$A_4 = \pi \Sigma \cos^2 2\theta_i$$

$$A_5 = 2\Sigma \sin 2\theta_i \cos 2\theta_i - 2 \Sigma (\pi f_i + 1) \cos 2\theta_i$$

and where Σ represents summation over the number of experimental data pairs, N.

A similar, but more lengthy, expression is obtained from

$$\frac{\partial V}{\partial \bar{\theta}} = 0$$

Solution can be obtained by simply substituting various values of $\bar{\theta}$ and plotting the resultant values of e until an intersection of the two curves is obtained, noting the restrictions that the derivation requires $e \leq 1.0$, and $0 \leq \bar{\theta} \leq \pi/2$.

C.3 Results Obtained From RSI Photomicrographs

The photomicrographs supplied to Materials Sciences Corporation by NASA/Langley have been studied and data taken to provide fiber distribution information. The scanning line technique was used as follows. A line 600 micrometers in length was taken as a fixed length. Angular orientations from -90 to +90 degress, in 15 degree increments were marked on the photographs. For each angular orientation, the scanning line was placed at twenty different locations on the photograph and the number of fibers which intersected the scanning line were counted. Thus, for each of twelve angular orientations, twenty readings of number of intersections were obtained in an effort to obtain representative numbers from each photograph. Fibers which could be identified through the stereo photos as being significantly out of the plane of the photograph were not included when totaling the number of fiber intersections. Since the angle which yields the most intersections implies that the primary fiber orientation is at ninety degrees to that angle, all angles were shifted ninety degrees to reflect the actual fiber orientation.

The resulting tables of data were then used to determine the best fit values of e and $\bar{\theta}$ for equation C-1. The results obtained from equation C-1 along with considering the fabrication process prompted fitting the data to equation C-7 since it was felt that this distribution function would be more realistic.

RSI MODEL RESULTS FOR TENSION LOADING
EFFECT OF ANGLE OF ORIENTATION OF FIBERS

TABLE B-I

Distribution Type of the Angle of Orientation of the Fibers	Ultimate Stress of the RSI Material MN/m^2 (PSI)
Fig. B-5 (a)	1.405 (204)
" " (b)	1.275 (185)
" " (c)	1.536 (223)
" " (d)	1.902 (276)
" " (e)	1.006 (146)
" " (f)	2.150 (312)
" " (g)	1.226 (178)
" " (h)	1.330 (193)

RSI MODEL RESULTS FOR TENSION LOADING
EFFECT OF FIBER STRENGTH DISTRIBUTION

TABLE B-II

Distribution Type of the Angle of Orientation of the Fiber	Strength Distribution Type of the Fiber	Ultimate Stress of RSI Model MN/m^2 (PSI)
Fig. B-5 (b)	Fig. B-7 (a)	1.275 (185)
" " (b)	" " (b)	.661 (96)
" " (b)	" " (c)	.696 (101)
" " (b)	" " (d)	.661 (96)
" " (b)	" " (e)	.785 (114)

RSI MODEL RESULTS FOR COMPRESSION LOADING
EFFECT OF ANGLE OF ORIENTATION OF FIBERS

TABLE B-III

Distribution Type Of The Angle Of Orientation Of The Fibers	Ultimate Stress of the RSI Material MN/m^2 (PSI)	
Fig. B-5 (a)	-1.350	(-196)
" " (b)	-1.233	(-179)
" " (c)	-1.481	(-215)
" " (d)	-1.826	(-265)
" " (e)	- .971	(-141)
" " (f)	-2.067	(-300)
" " (g)	-1.213	(-176)
" " (h)	-1.281	(-186)

RSI MODEL RESULTS FOR COMPRESSION LOADING
EFFECT OF FIBER STRENGTH DISTRIBUTION

TABLE B-IV

Distribution Type Of The Angle of Orientation Of The Fibers	Strength Distribution Type of Fiber	Ultimate Stress of the RSI Material MN/m^2 (PSI)	
Fig. B-5 (b)	Fig. B-7 (a)	-1.233	(-179)
" " (b)	" " (b)	- .648	(- 94)
" " (b)	" " (c)	- .668	(- 97)
" " (b)	" " (d)	- .586	(- 85)
" " (b)	" " (e)	- .772	(-112)

RSI MODEL RESULTS FOR SHEAR LOADING
EFFECT OF ANGLE OF ORIENTATION OF FIBERS

TABLE B-V

Distribution Type Of The Angle Of Orientation Of The Fibers	Ultimate Stress of the RSI Material MN/m^2	(PSI)
Fig. B-5 (a)	1.254	(182)
" " (b)	1.357	(197)
" " (c)	1.302	(189)
" " (d)	.572	(83)
" " (e)	.854	(124)
" " (f)	.675	(98)
" " (g)	1.709	(248)
" " (h)	.999	(145)

RSI MODEL RESULTS FOR SHEAR LOADING
EFFECT OF FIBER STRENGTH DISTRIBUTION

TABLE B-VI

Distribution Type of the Angle of Orientation of the Fibers	Strength Distribution Type of Fiber	Ultimate Stress of the RSI Material MN/m^2 (PSI) Results For Initial Fiber Strength Assignments	Results For Revising Order of Fiber Strength Assignments
Fig.B-5 (b)	Fig.B-7 (a)	1.357 (197)	1.357 (197)
" " (b)	" " (b)	1.158 (168)	.937 (136)
" " (b)	" " (c)	1.089 (158)	.923 (134)
" " (b)	" " (d)	1.075 (156)	.902 (131)
" " (b)	" " (e)	1.309 (190)	1.054 (153)

RSI MODEL RESULTS FOR COMBINED
TENSION AND SHEAR LOADING
EFFECT OF ANGLE OF ORIENTATION OF FIBERS

TABLE B-VII

Distribution Type Of The Angle Of Orientation Of Fibers	Ultimate Stress of the RSI Material MN/m^2	(PSI)
Fig. B-5 (a)	.827	(120)
" " (b)	.820	(119)
" " (c)	.847	(123)
" " (d)	.482	(70)
" " (e)	.537	(78)
" " (f)	.558	(81)
" " (g)	1.206	(175)
" " (h)	1.247	(181)

RSI MODEL RESULTS FOR COMBINED
TENSION AND SHEAR LOADING
EFFECT OF FIBER STRENGTH DISTRIBUTION

TABLE B-VIII

Distribution Type Of The Angle Of Orientation Of Fibers	Strength Distribution Type Of The Fiber	Ultimate Stress of the RSI Material MN/m^2	(PSI)
Fig. B-5 (b)	Fig. B-7 (a)	.820	(119)
" " (b)	" " (b)	.441	(64)
" " (b)	" " (c)	.427	(62)
" " (b)	" " (d)	.400	(58)
" " (b)	" " (e)	.530	(77)

RSI MODEL RESULTS FOR THERMAL LOADING ON MODEL IN FIG. 13, GIVEN INITIAL THERMAL STRAINS AND APPLIED TENSION LOADING

TABLE B-IX

Distribution Type Of The Angle Of Orientation Of Fibers	Initial Strains ε°_{11} And ε°_{22} Applied In The 1 And 2 Directions	Ultimate Stress of RSI Material In Tension MN/m^2 (PSI)
Fig. B-5 (b)	0	1.275 (185)
" " (b)	0.000424	1.254 (182)
" " (b)	0.000784	1.240 (180)
" " (b)	0.001144	1.226 (178)
" " (b)	0.001504	1.213 (176)
" " (b)	0.001864	1.199 (174)

RSI MODEL RESULTS FOR THERMAL LOADING ON MODEL IN FIG. 13, GIVEN INITIAL THERMAL STRAINS AND COMBINED TENSION AND SHEAR LOADING APPLIED

TABLE B-X

Distribution Type Of The Angle Of Orientation Of Fibers	Initial Strains ε°_{11} And ε°_{22} Applied In The 1 And 2 Directions	Ultimate Stress of RSI Material In Tension MN/m^2 (PSI)
Fig. B-5 (b)	0	.820 (119)
" " (b)	0.000424	.806 (117)
" " (b)	0.000784	.785 (114)
" " (b)	0.001144	.772 (112)
" " (b)	0.001504	.751 (109)
" " (b)	0.001864	.730 (106)

TABLE C-I

Values of ϕ_i for Representation of $f(\theta)$ at e = 0.95

ϕ_i \ N	2	4	6	8	10	12	16	20
1	33.96	8.52	5.54	4.19	3.40	2.88	2.22	1.93
2		47.26	22.44	16.32	12.94	10.75	8.08	6.60
3			54.08	30.37	23.30	19.07	14.10	11.36
4				58.36	35.72	28.34	20.47	16.28
5					61.38	39.70	27.41	21.45
6						63.65	35.35	27.01
7							45.34	33.18
8							66.93	40.35
9								49.56
10								70.11
α =	.3773	.3467	.3502	.3569	.3639	.3703	.3819	.4156

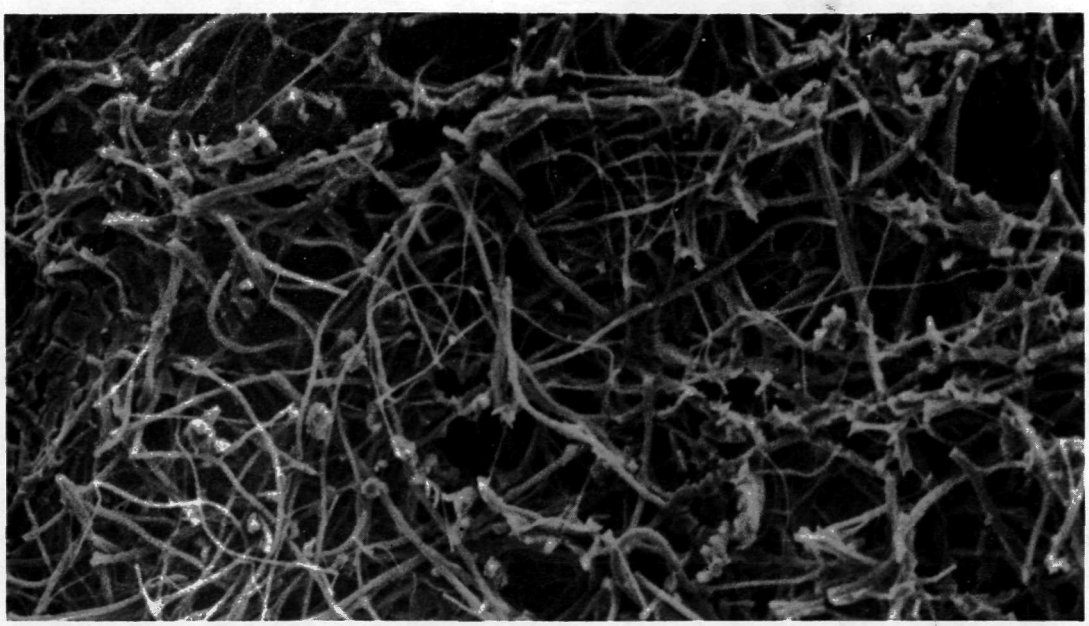

A) Small Diameter Fiber Material - RSI-SDF
Magnification: 200 X

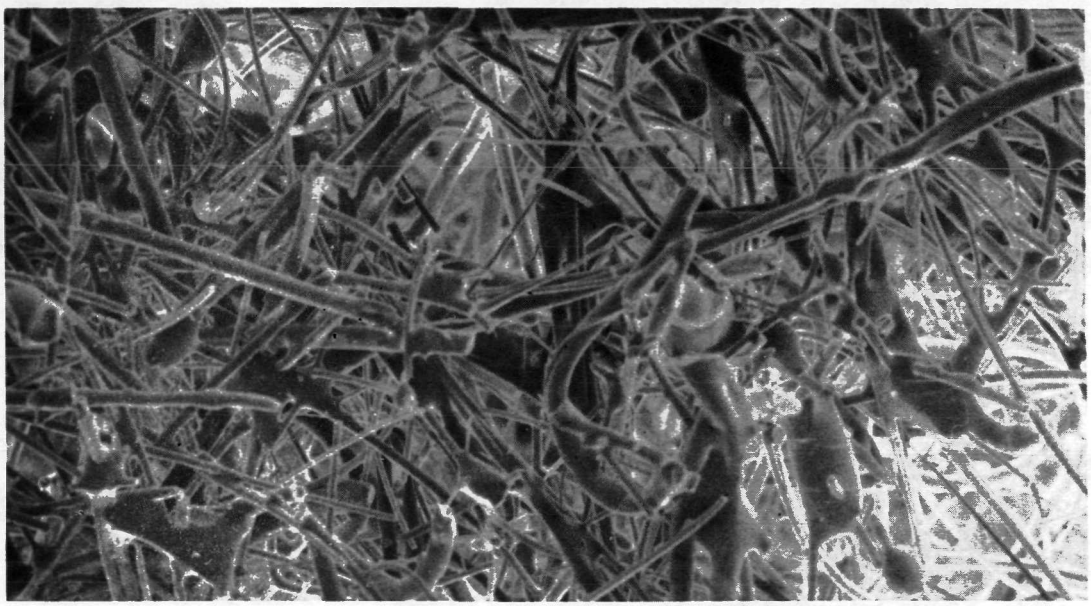

B) Large Diameter Fiber Material - RSI-LDF
Magnification: 100 X

Figure 1- Typical RSI Photomicrographs

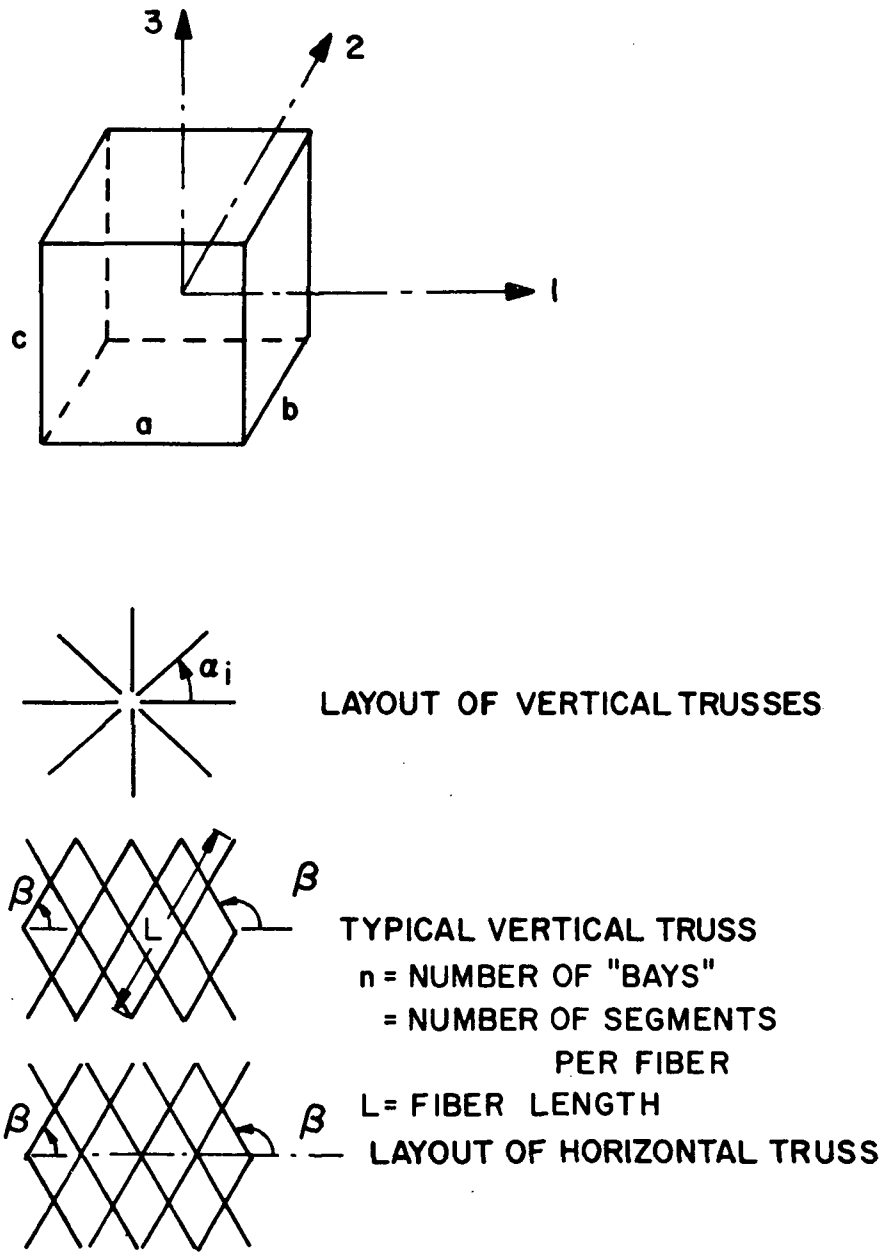

Figure 2 - A typical space model.

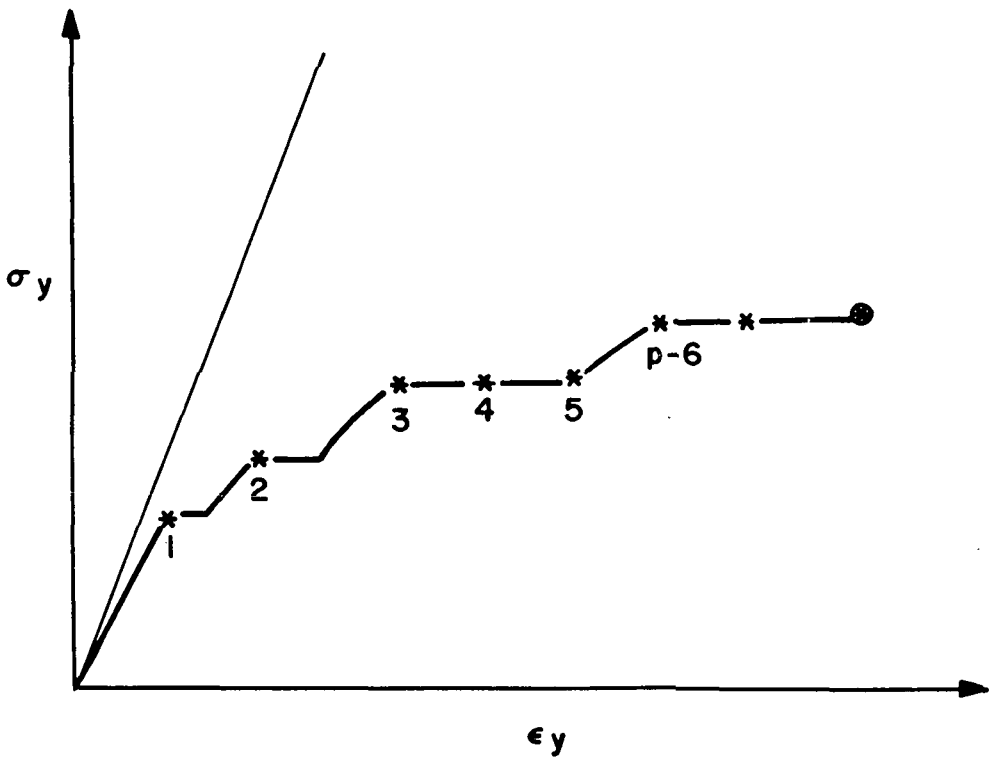

Figure 3 - Typical stress-strain behavior of a space model. Cross signs indicate the failure of trusses. Unstable situation occurred after the failure of p=6 number of trusses.

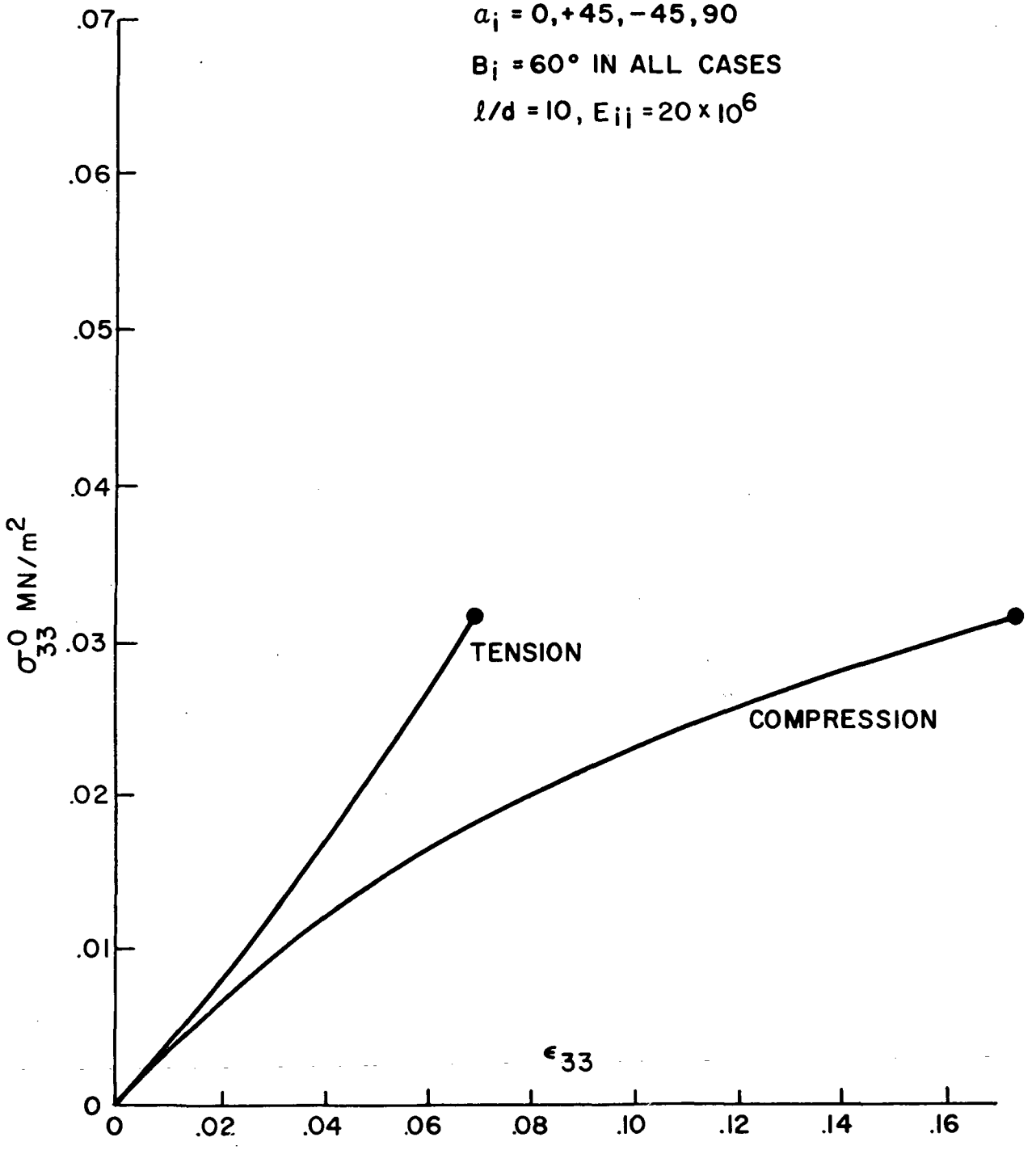

Figure 4 - Stress-strain behavior of a truss model under axial tension or compression (eccentricity of the fibers = 1.0).

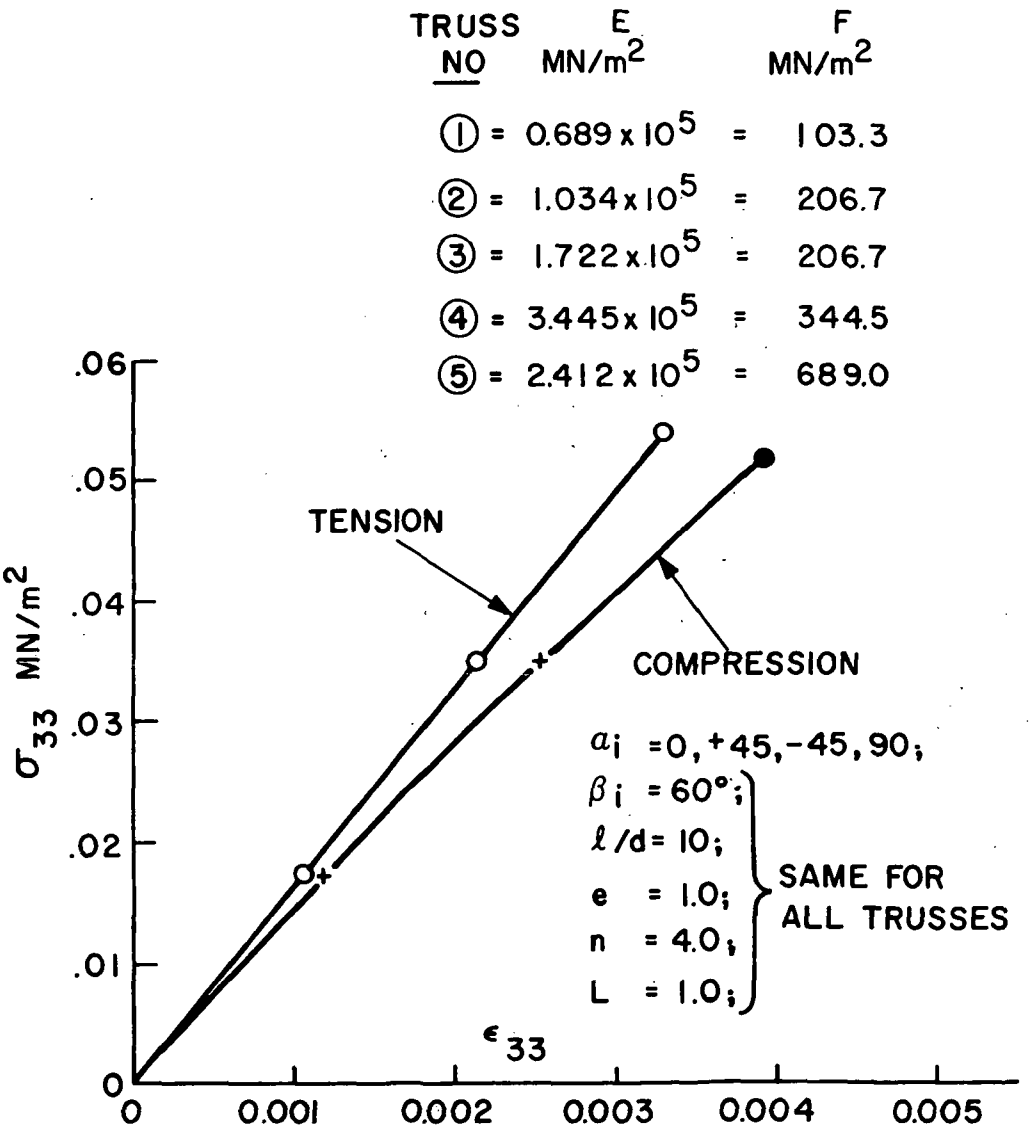

Figure 5 - Stress-strain behavior of the model under tension and compression.

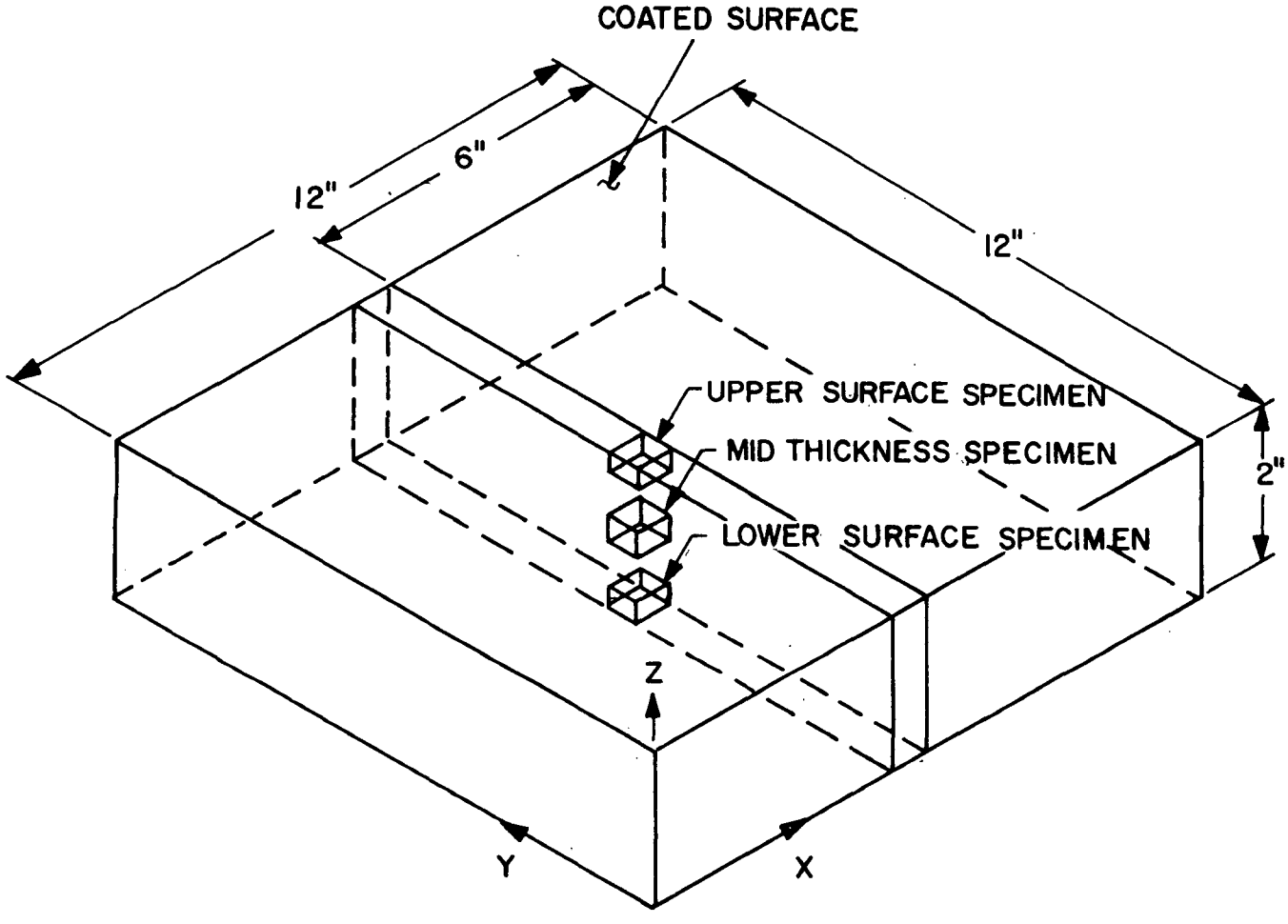

Figure 6 - Position and orientation of SEM specimens in contractor supplied RSI tiles.

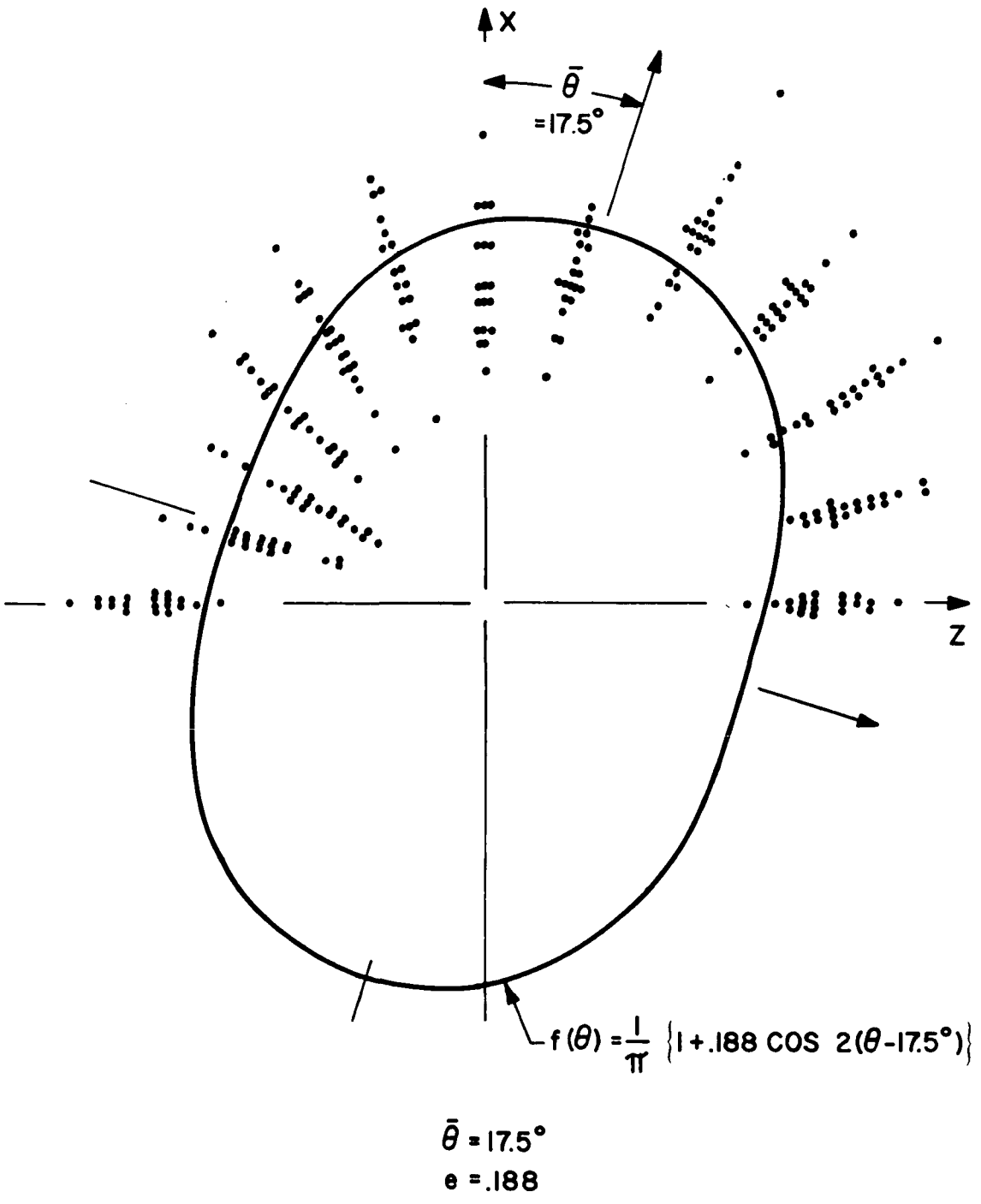

Figure 7 - Fiber distribution data for RSI -LDF - X-Z Plane

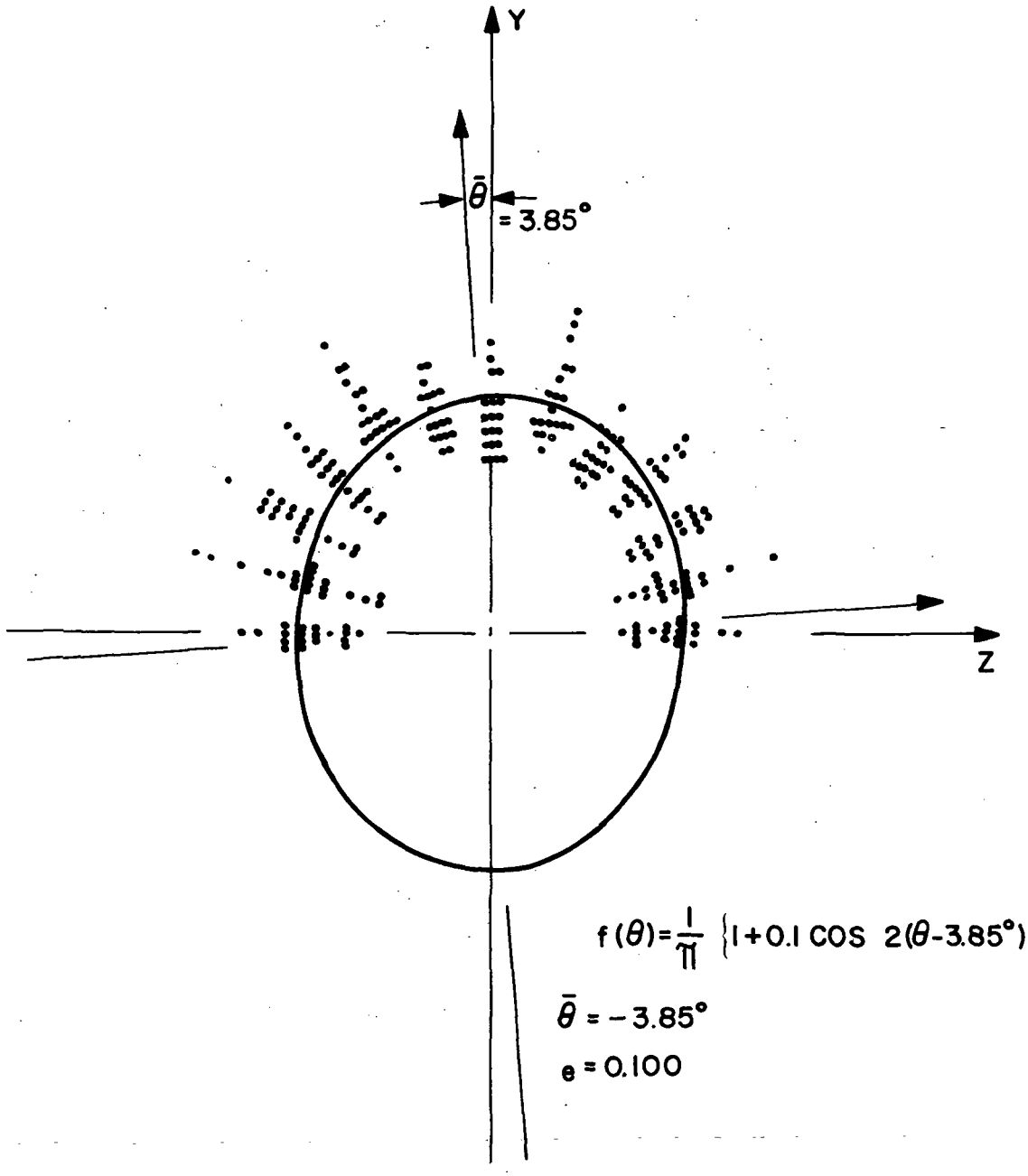

Figure 8 - Fiber distribution data for RSI -LDF - Y-Z Plane

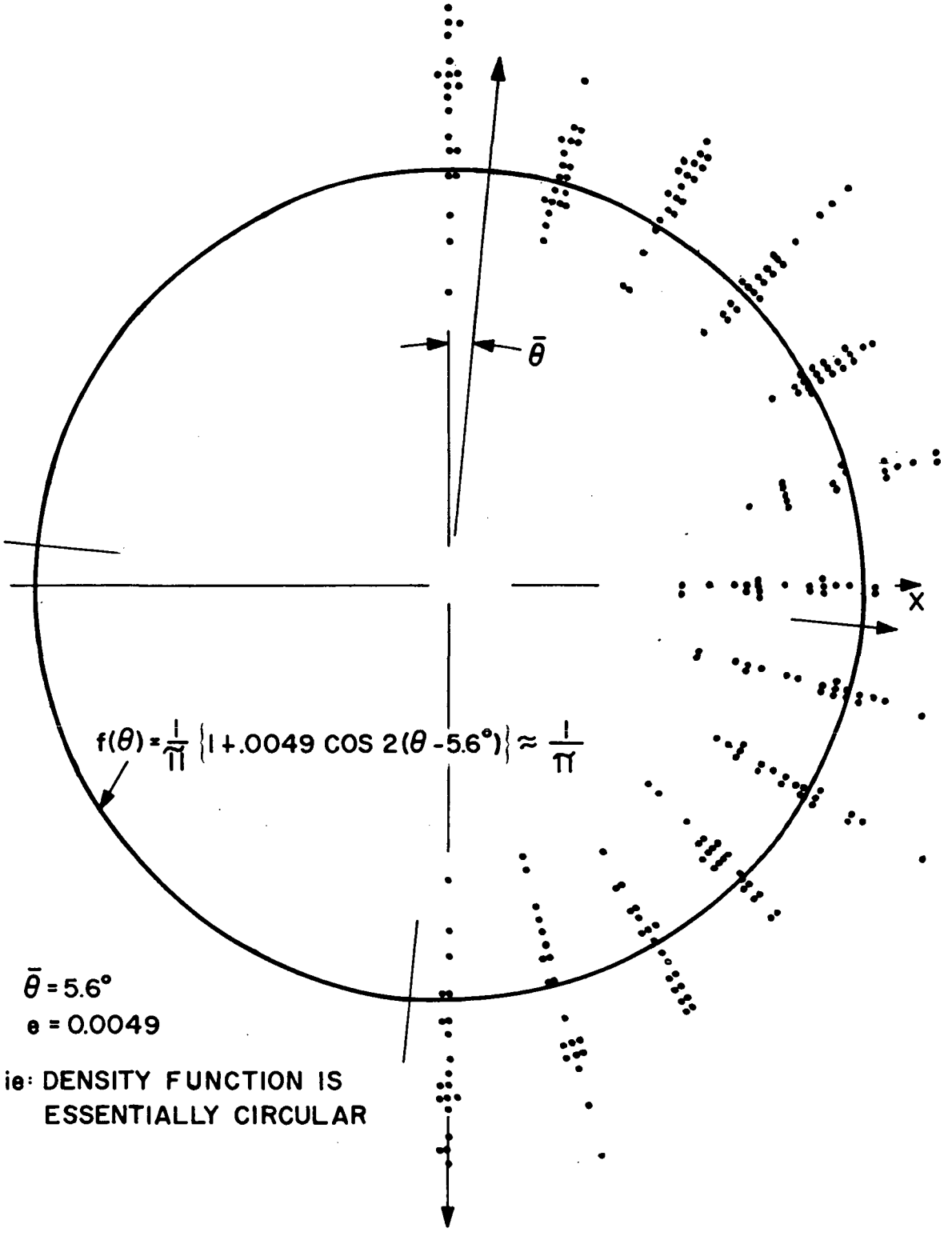

Figure 9 - Fiber distribution data for RSI-LDF - X-Y Plane

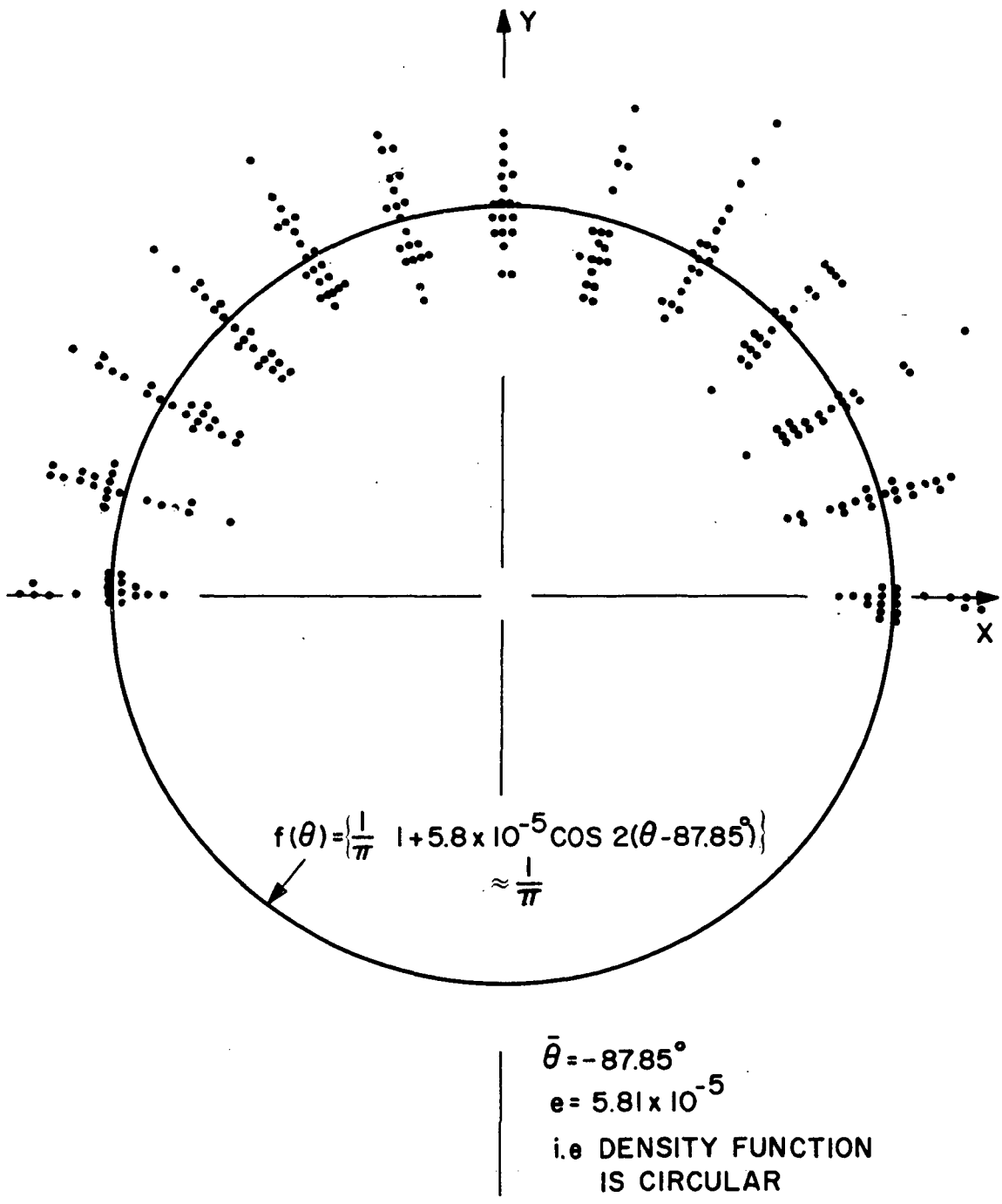

Figure 10 - Fiber distribution data for RSI-SDF- X-Y Plane.

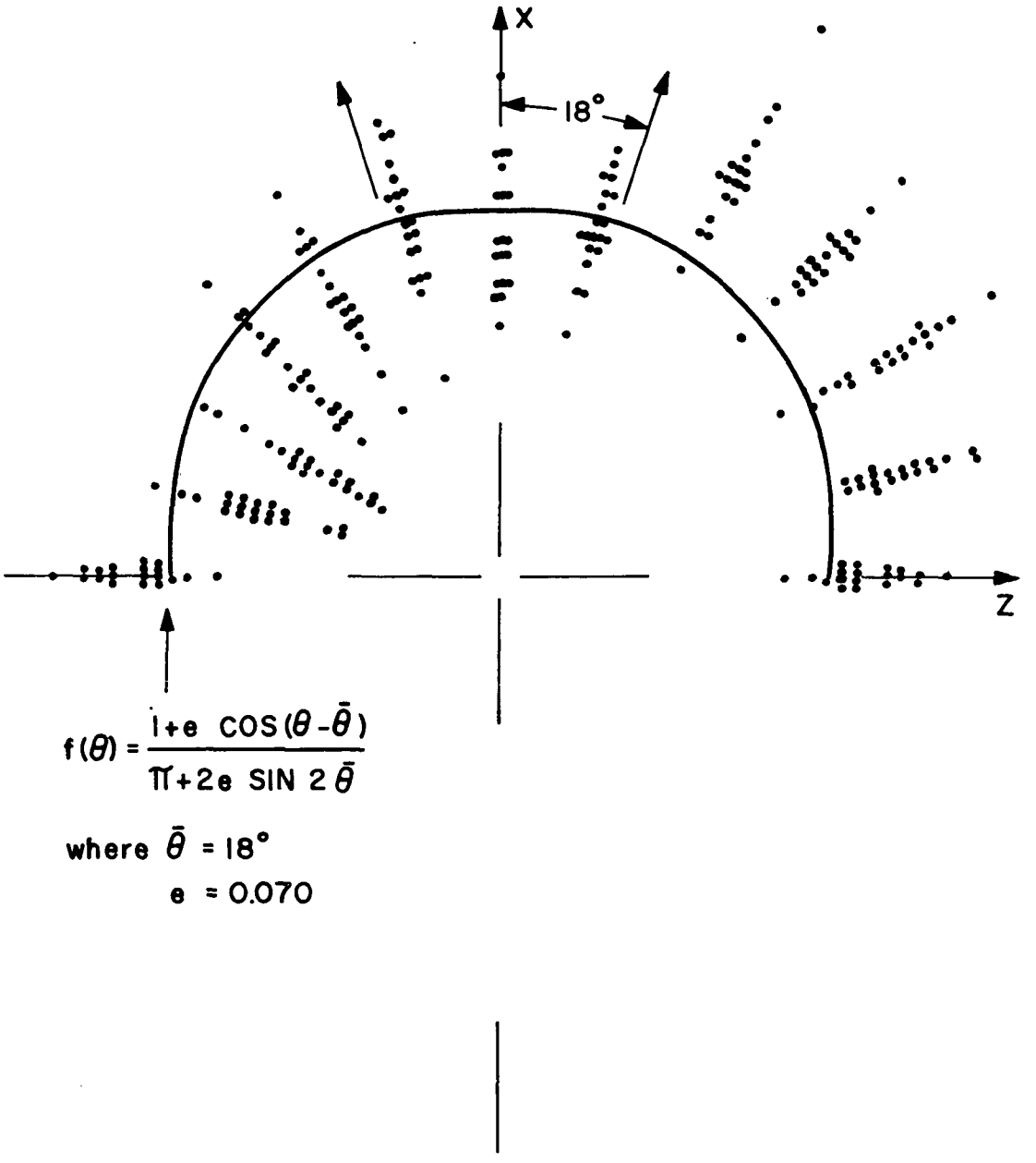

Figure 11 - Fiber distribution data and best fit elliptical distribution for RSI -LDF - X-Z Plane

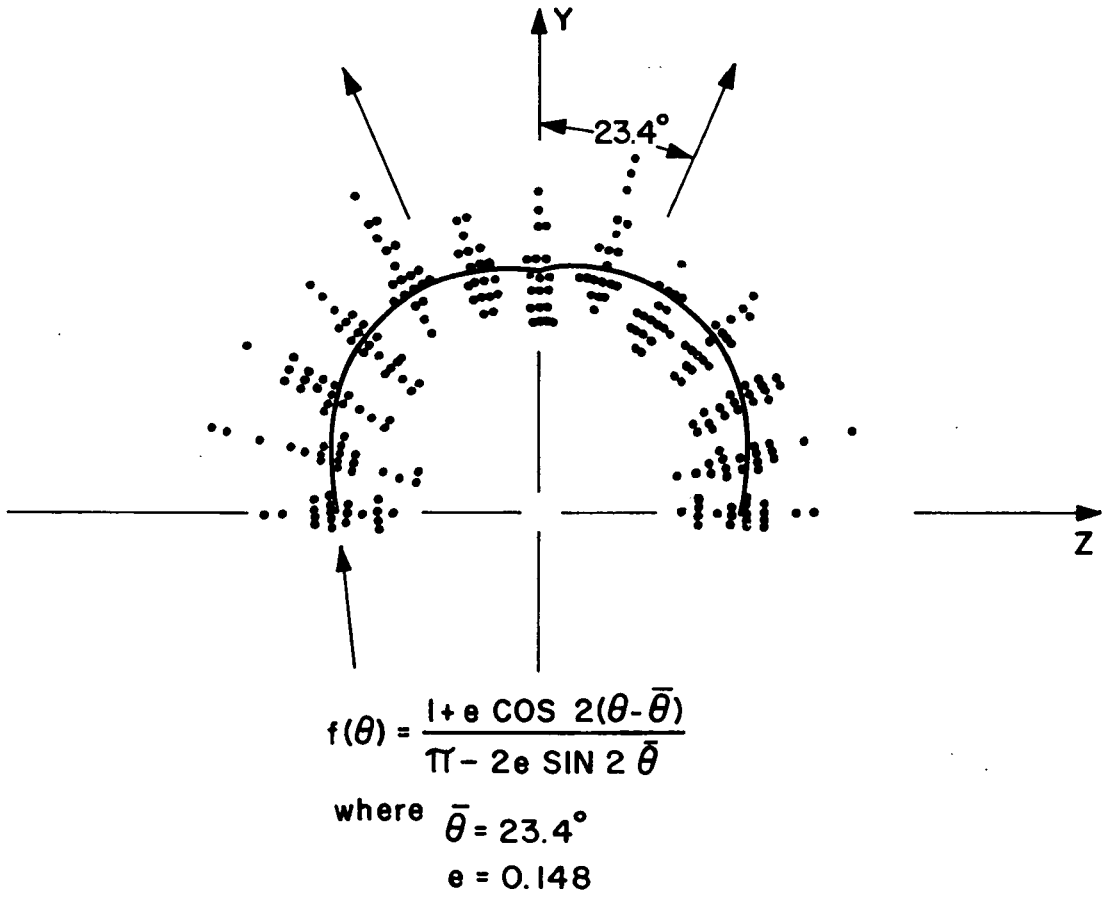

Figure 12 - Fiber distribution data for best fit elliptical distribution for RSI-LDF - Y-Z Plane

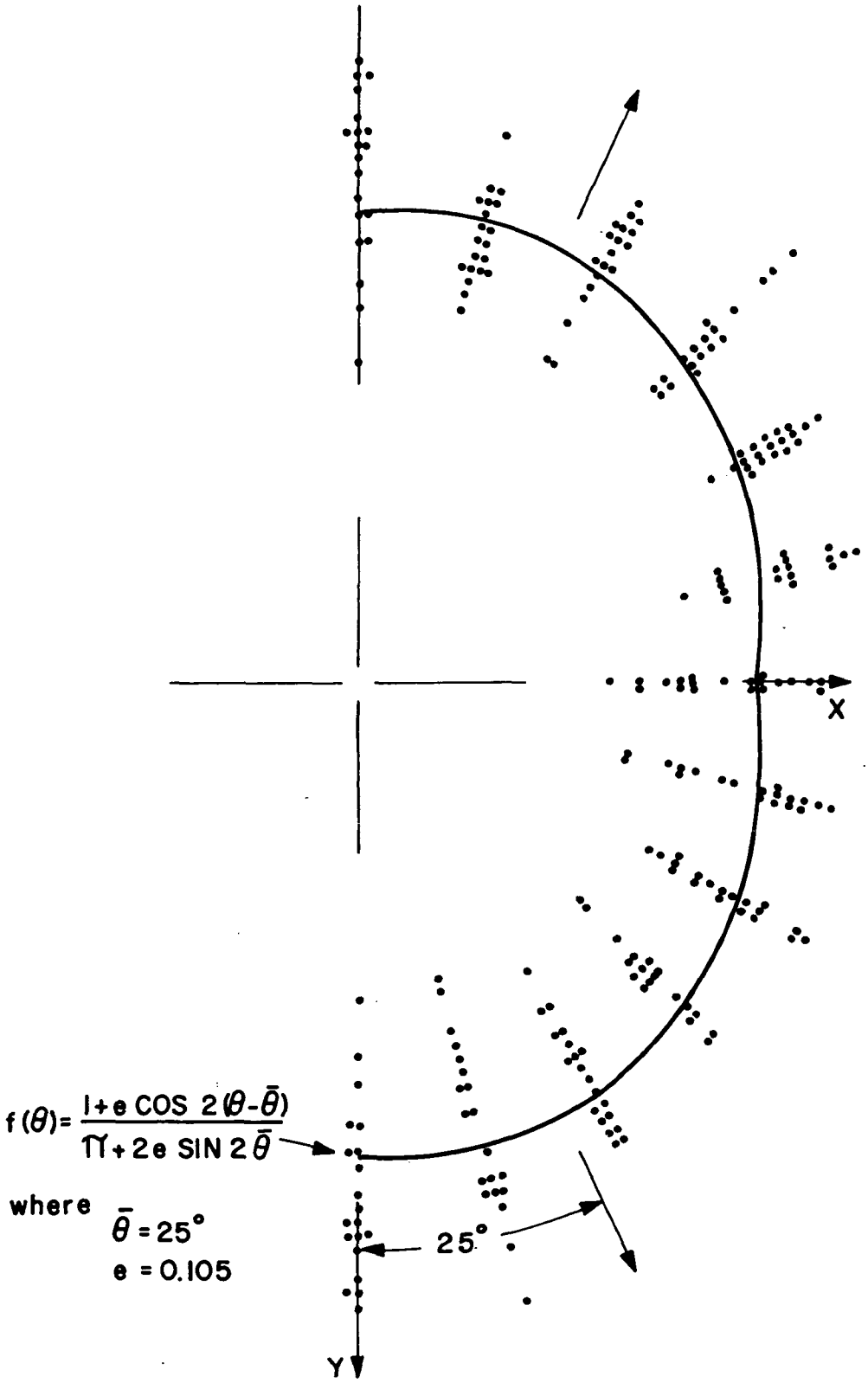

Figure 13 - Fiber distribution data and best fit elliptical distribution for RSI-LDF - X-Y Plane

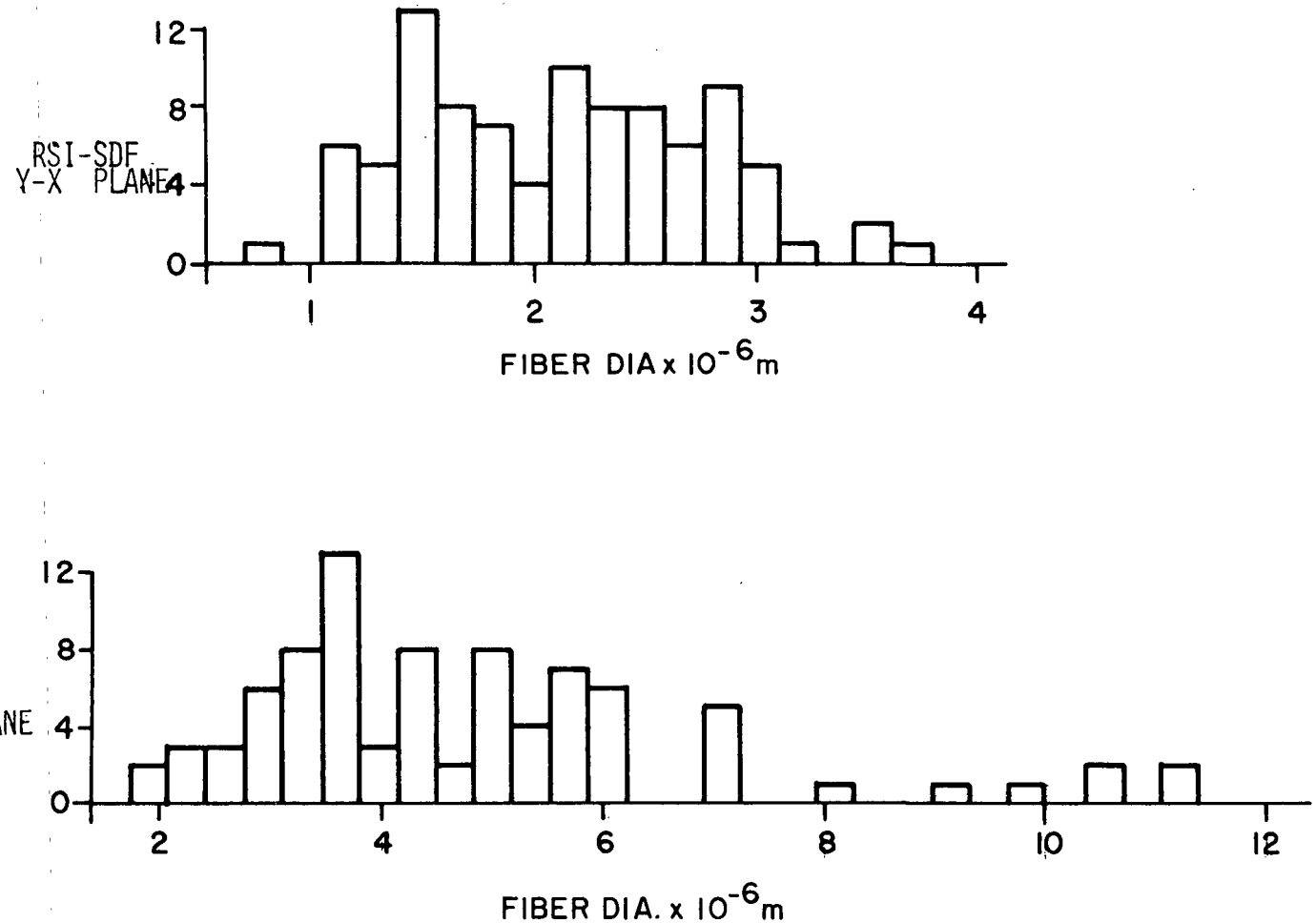

Figure 14 - Fiber Diameter Variation
a) RSI-SDF X-Y Plane
b) RSI-LDF - X-Y Plane

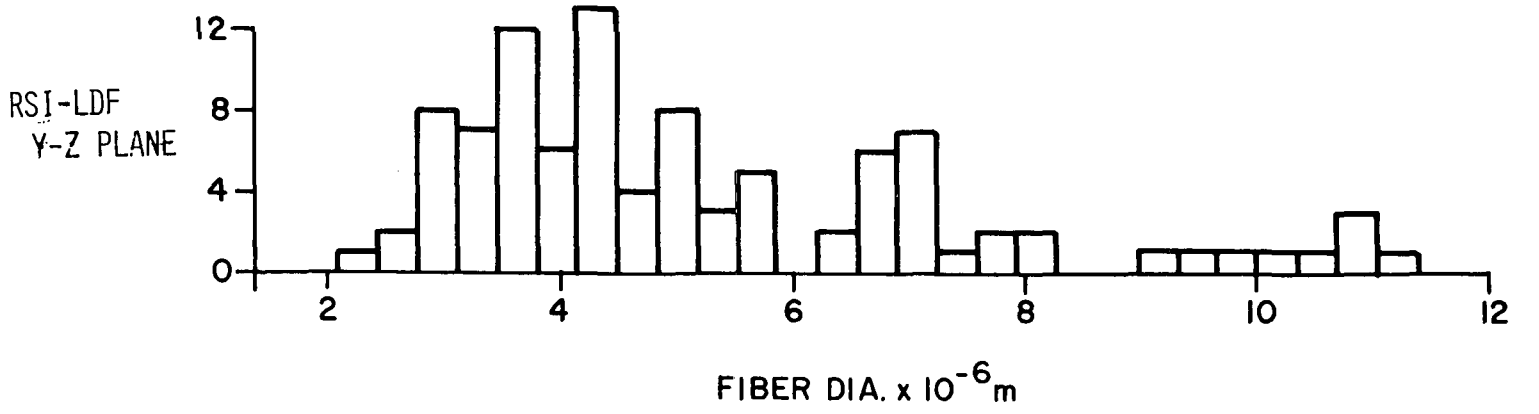

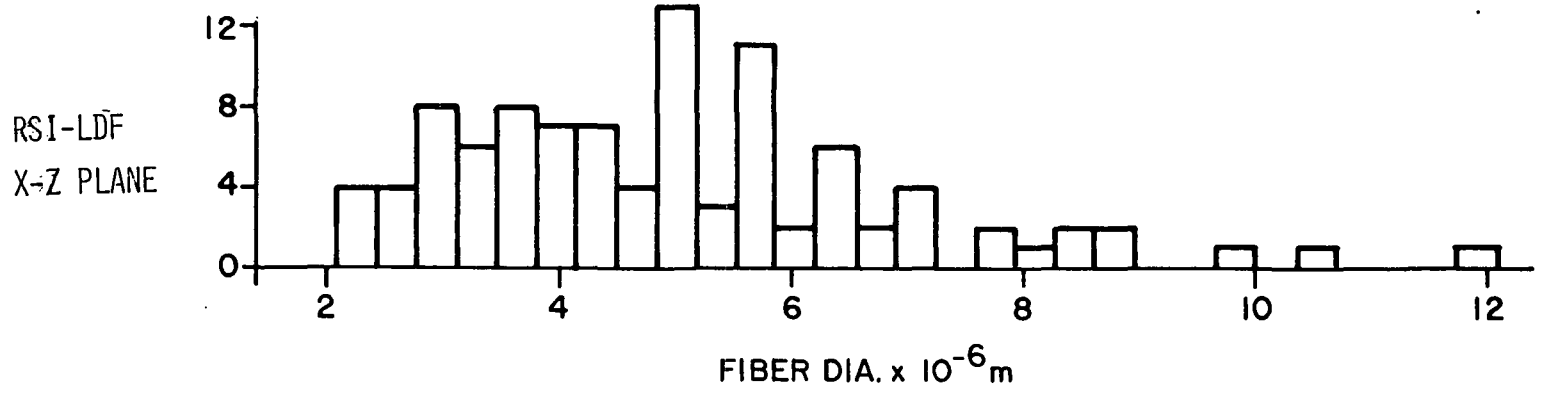

Figure 15 - Fiber Diameter Variation
a) RSI-LDF - Y-Z Plane
b) RSI-LDF - X-Z Plane

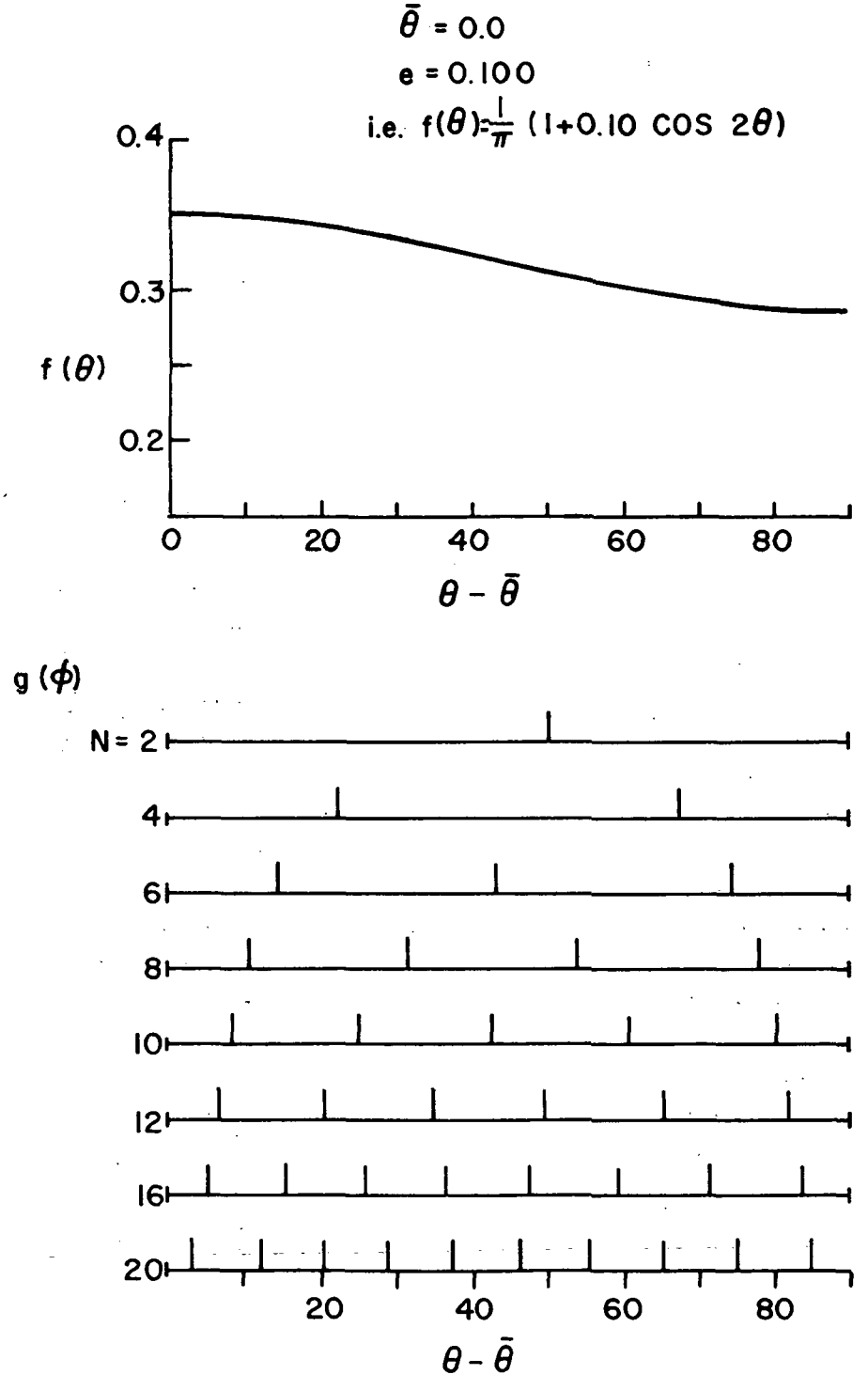

Figure 16 - Discrete fibers required to represent f(θ).

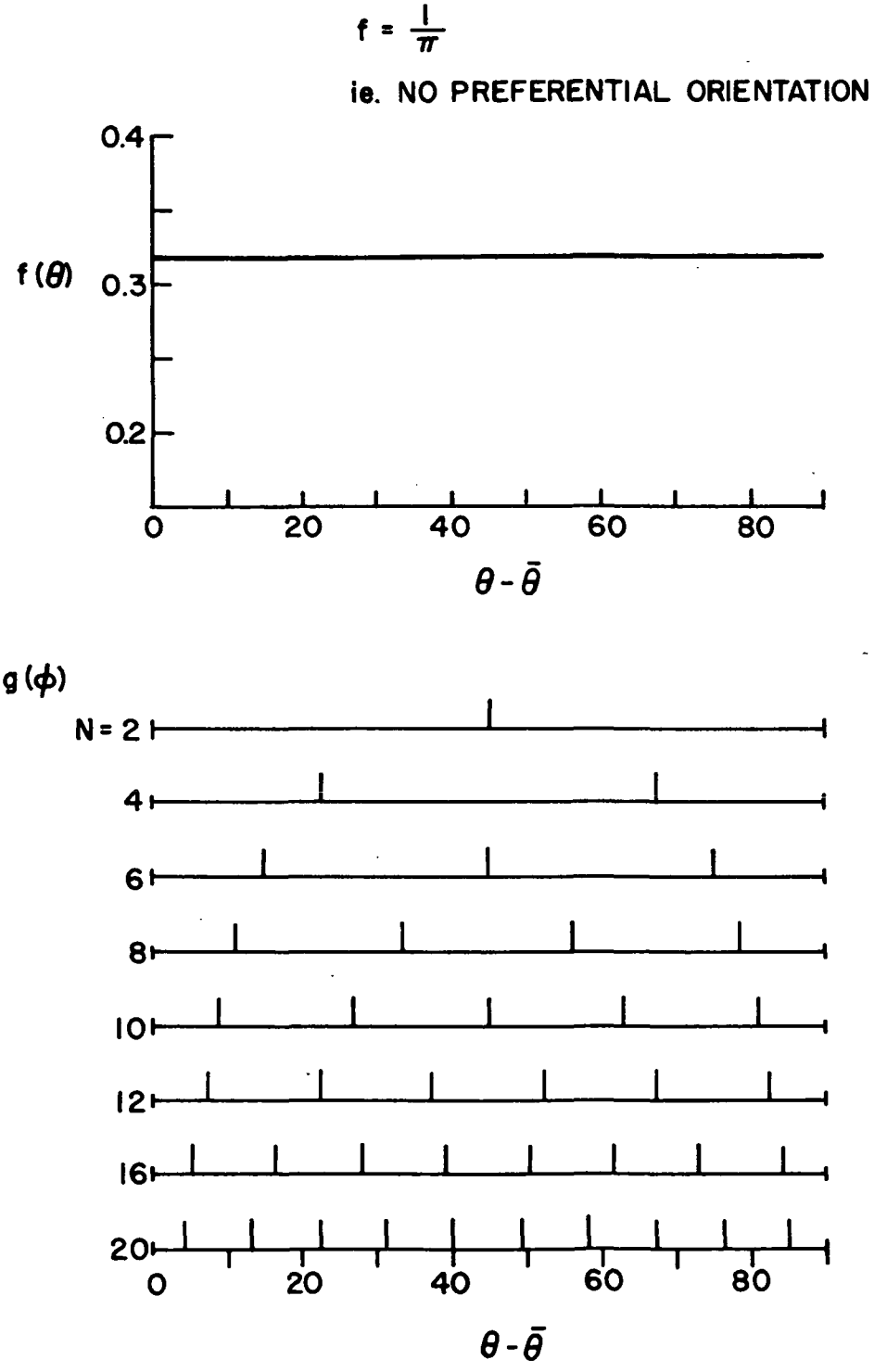

Figure 17 - Discrete fibers required for a uniform distribution.

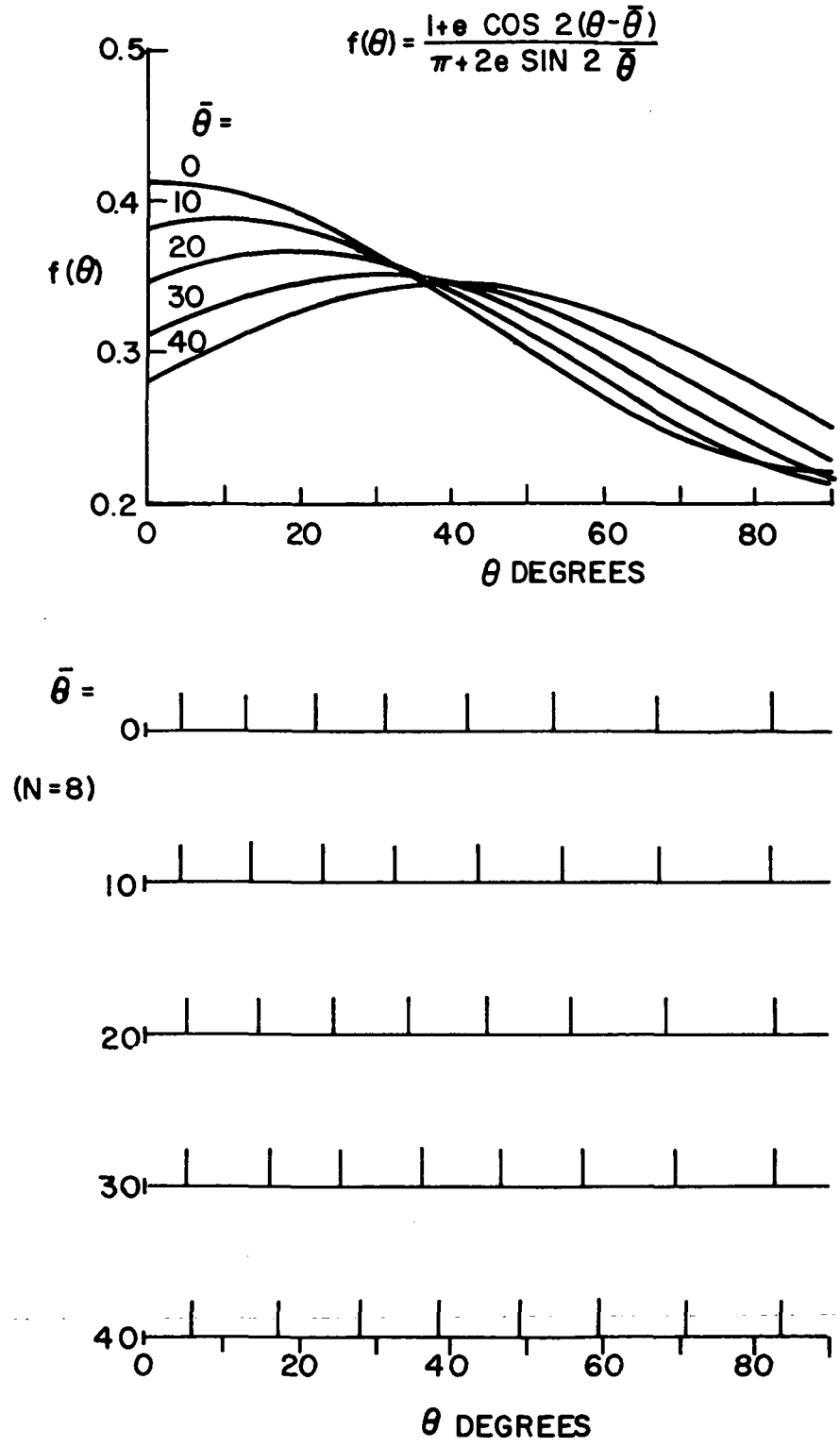

Figure 18 - Effect of $\bar{\theta}$ on fiber distribution for eccentricity = 0.30

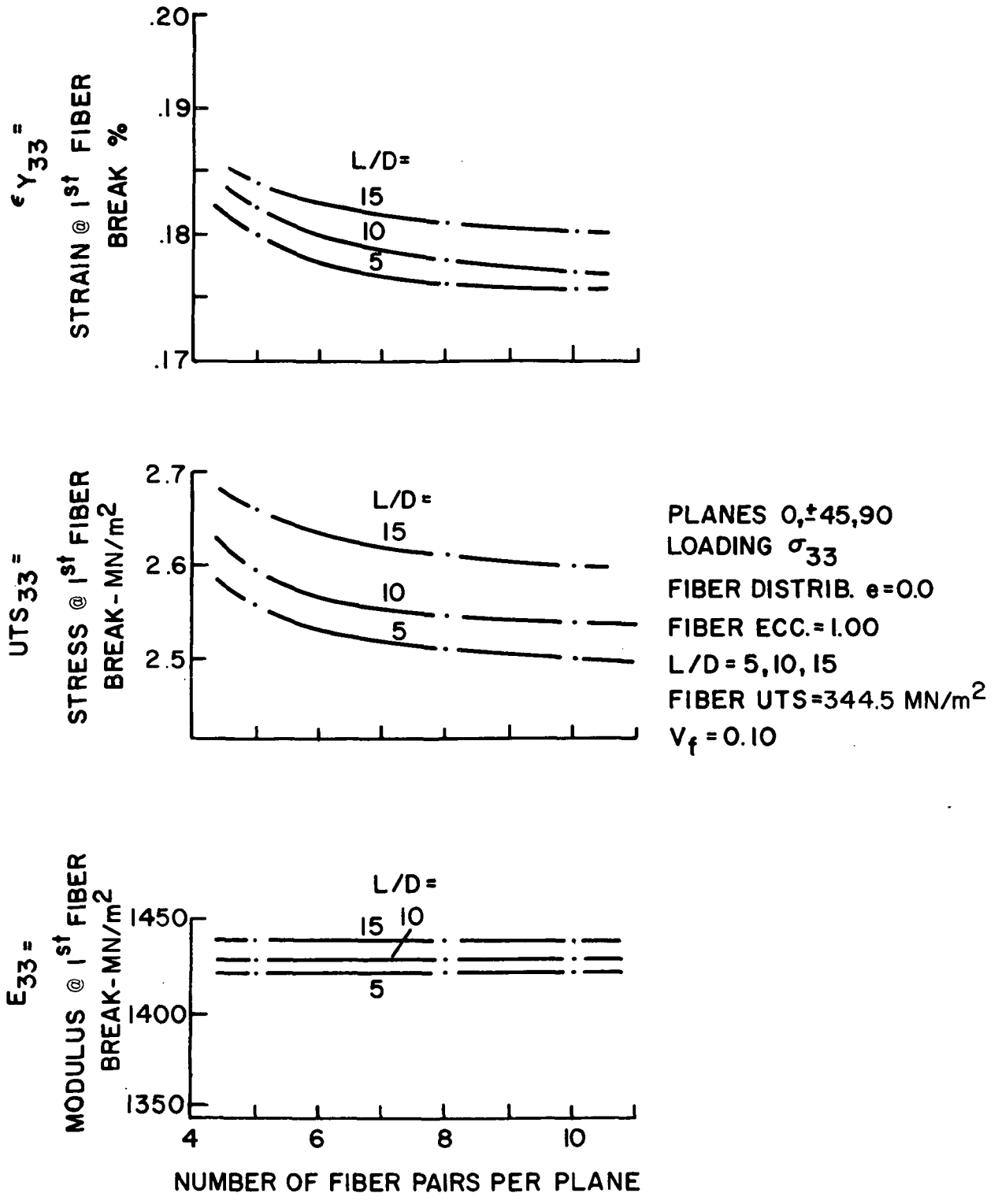

Figure 19 - Effect of the number of fiber pairs/plane on analysis results.

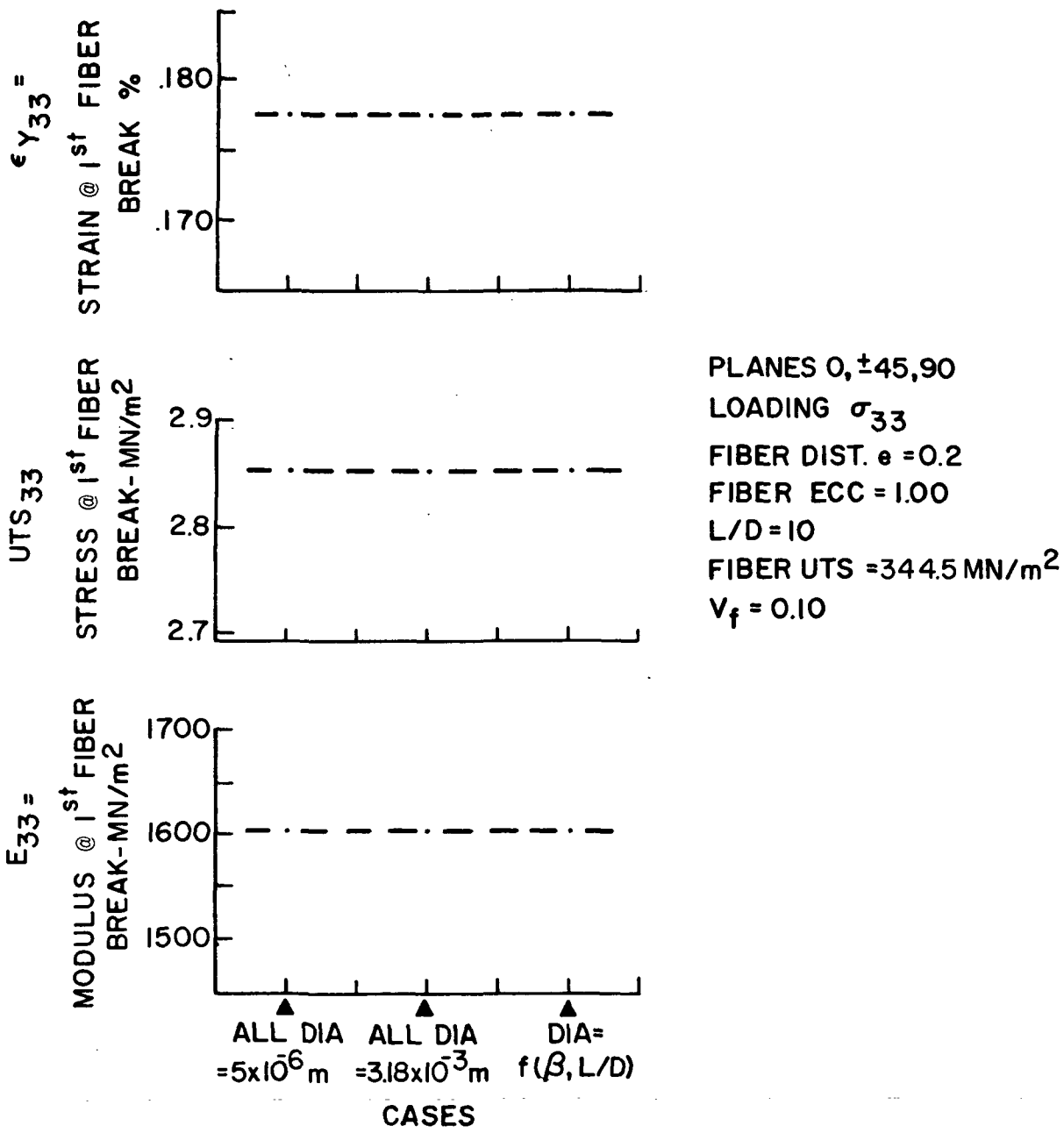

Figure 20 - Effect of varing fiber diameter while holding fiber L/D constant.

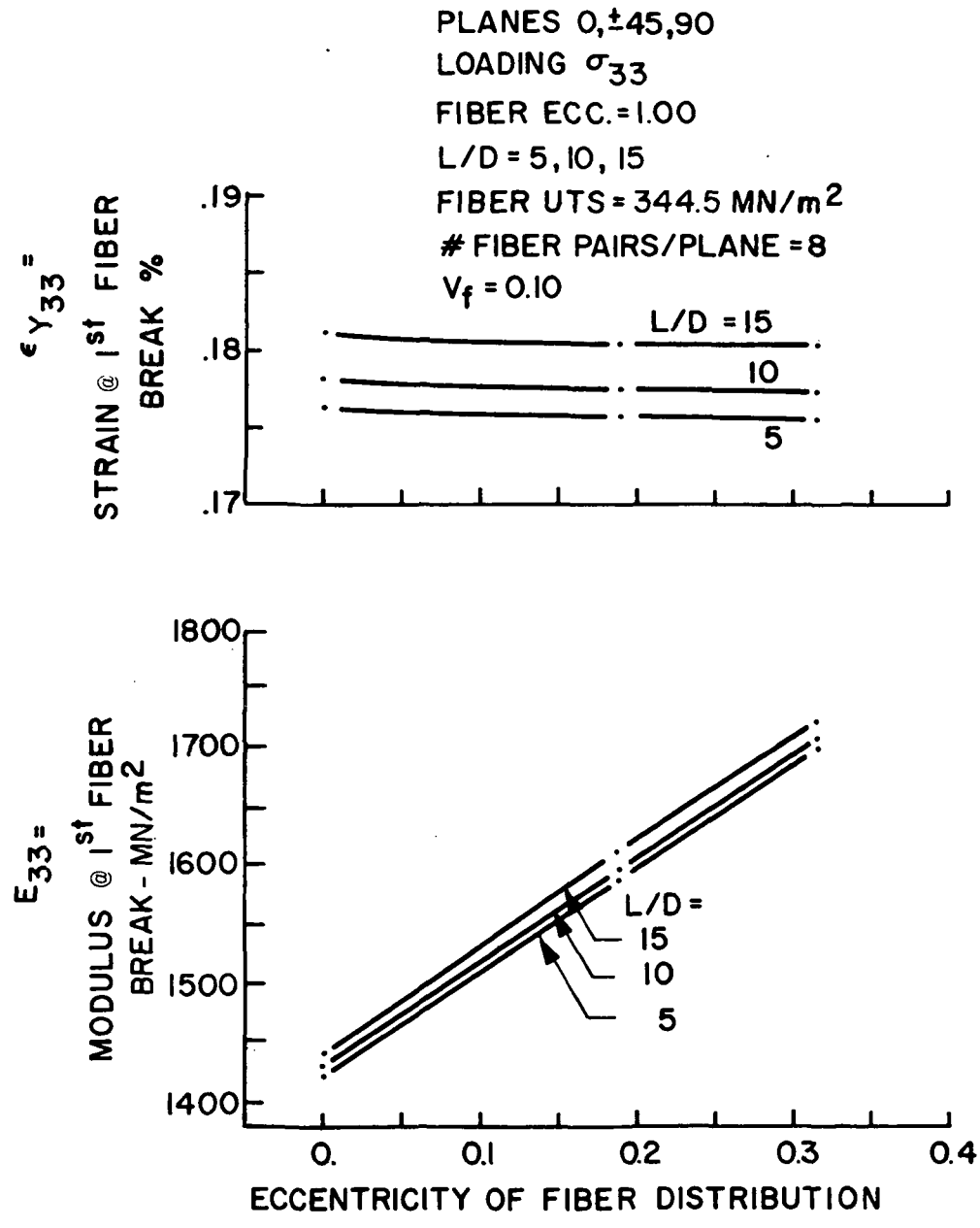

Figure 21 - Effect of eccentricity of fiber distribution on properties, $\bar{\theta}$ = 0.0

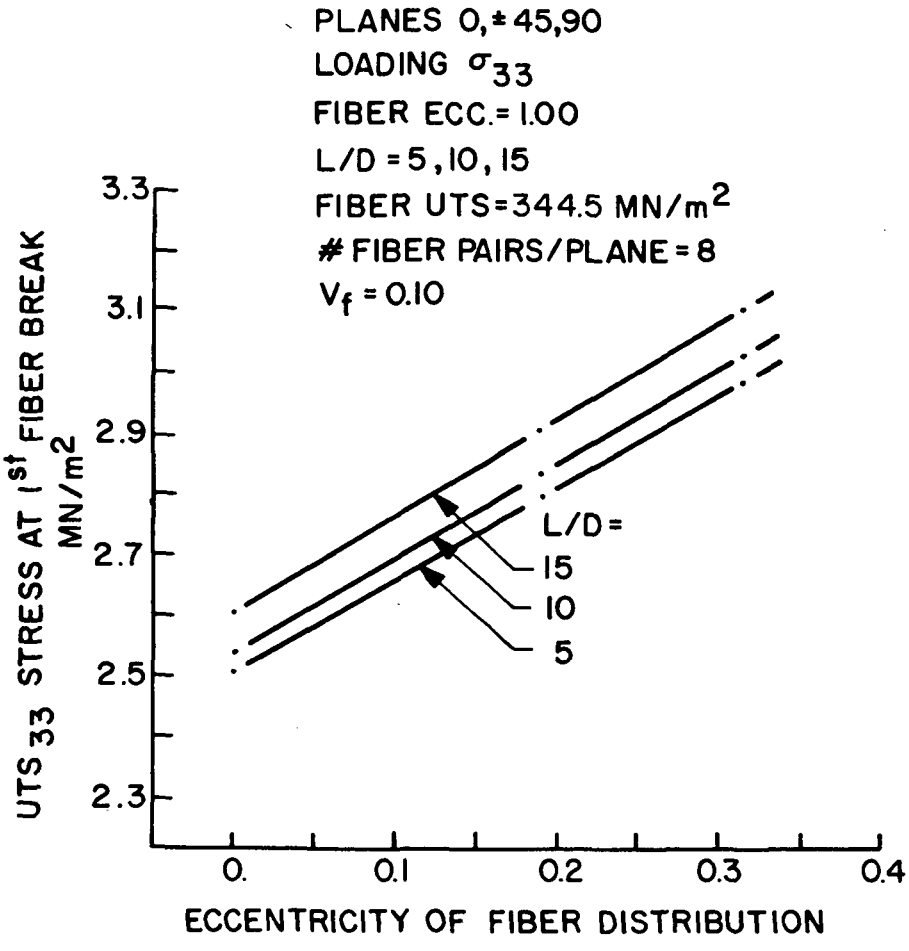

Figure 22 - Effect of eccentricity of fiber distribution on strength, $\bar{\theta}$ = 0.0

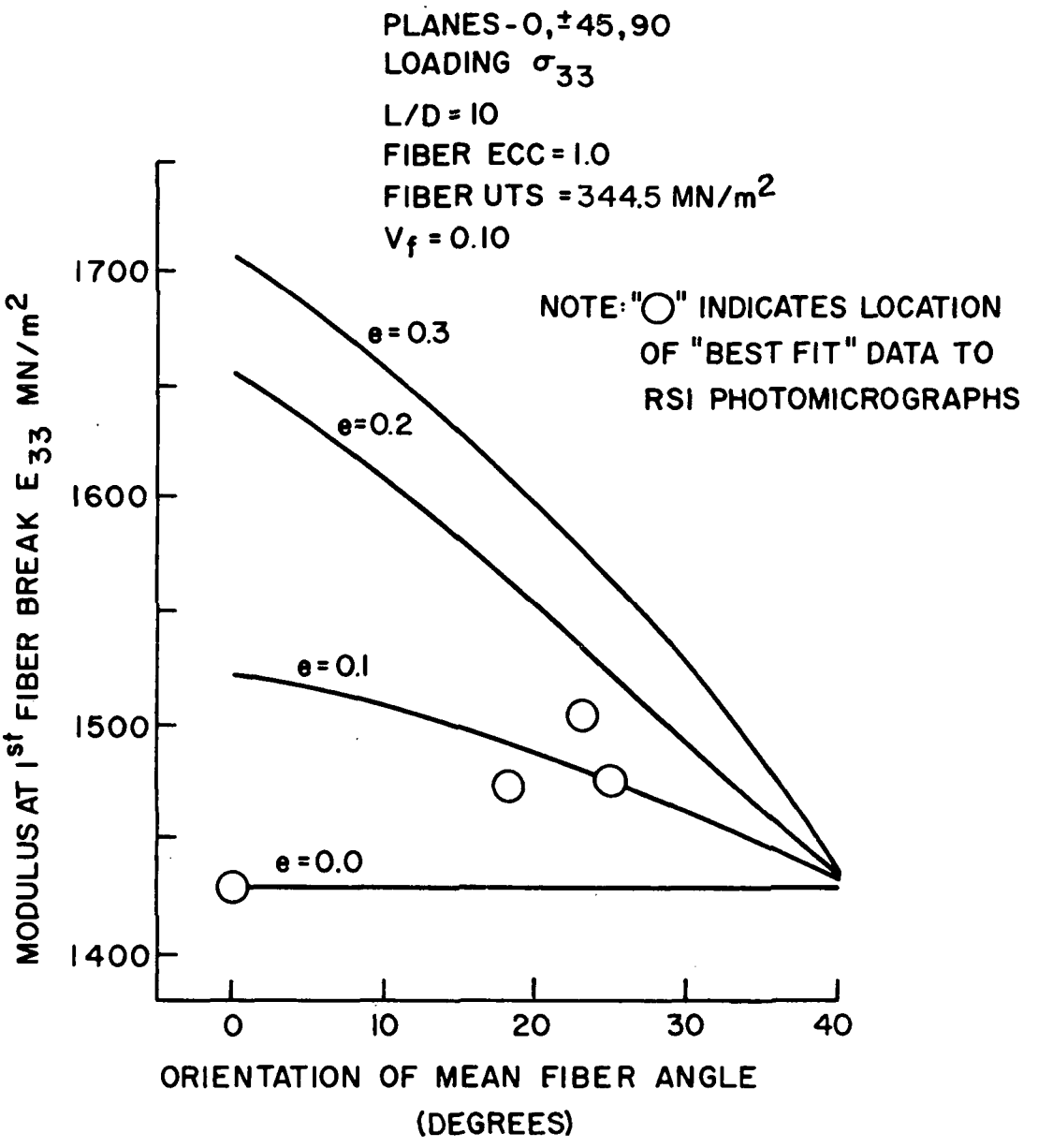

Figure 23 - Effect of orientation of fiber distribution on modulus of elasticity.

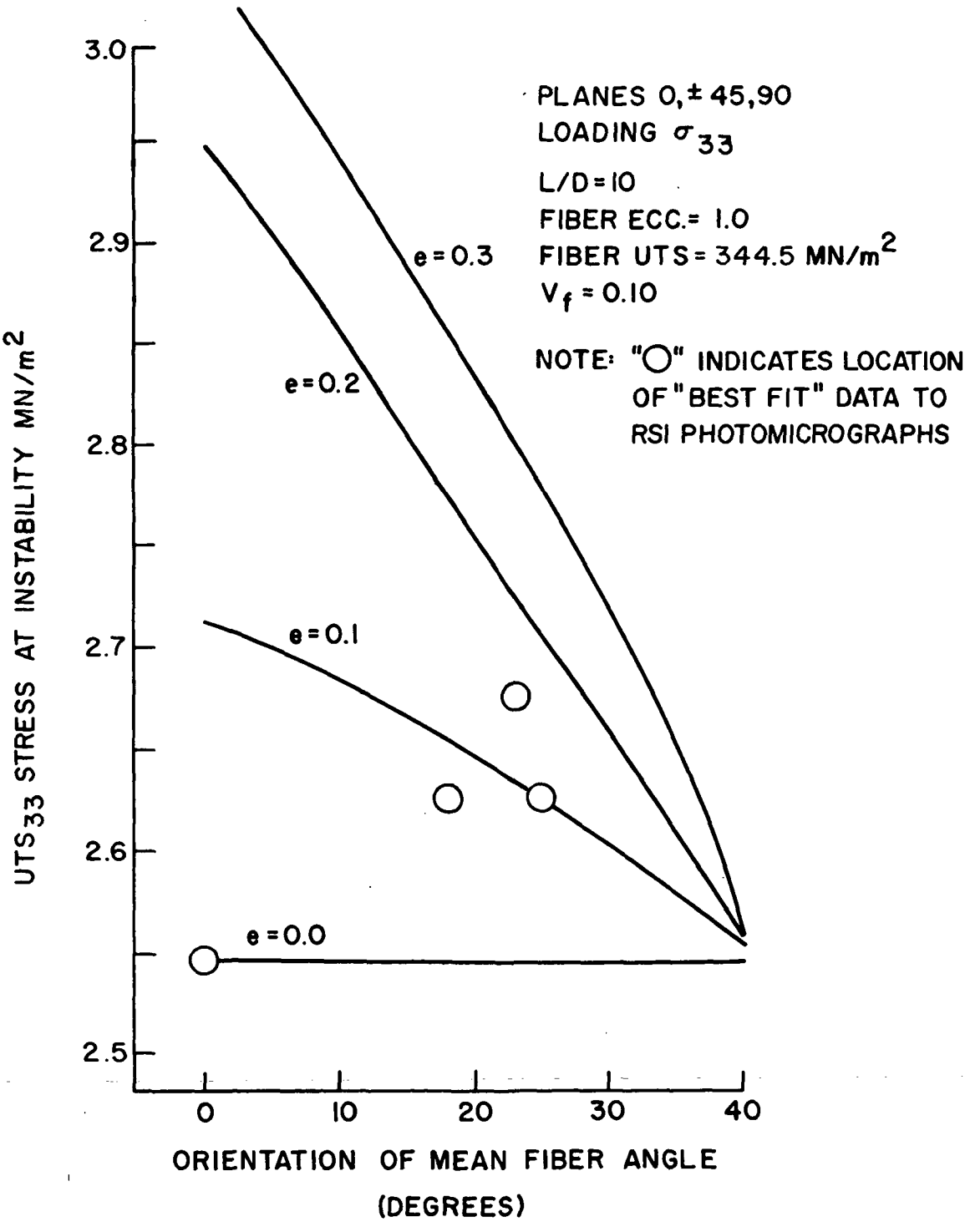

Figure 24 - Effect of orientation of fiber distribution on strength.

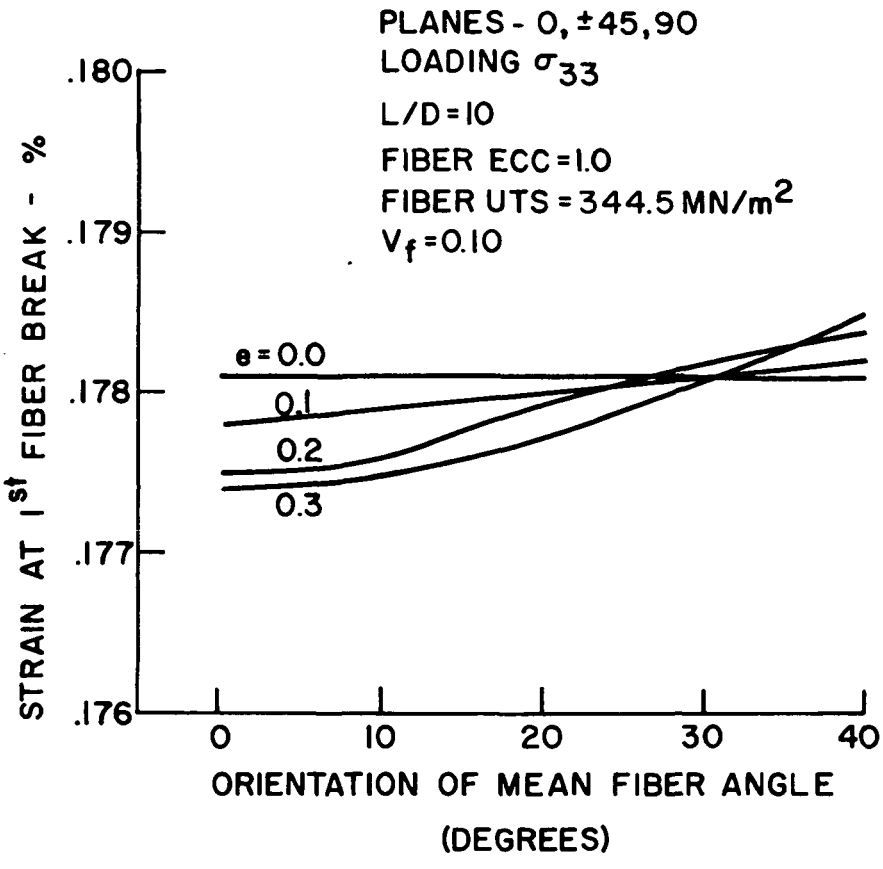

Figure 25 - Effect of orientation of fiber distribution on strain at first fiber break.

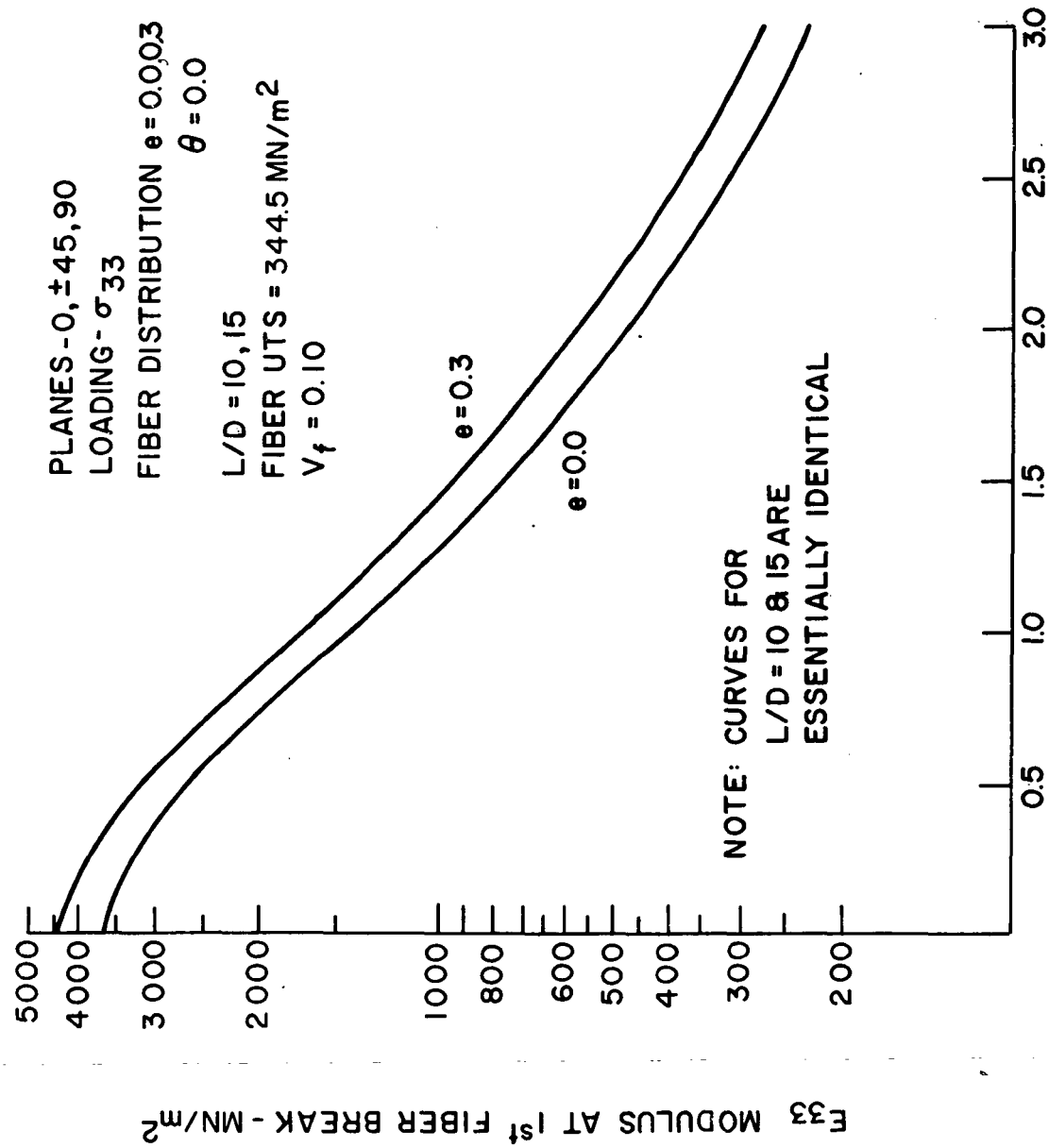

Figure 26 - Effect of fiber eccentricity on modulus of elasticity.

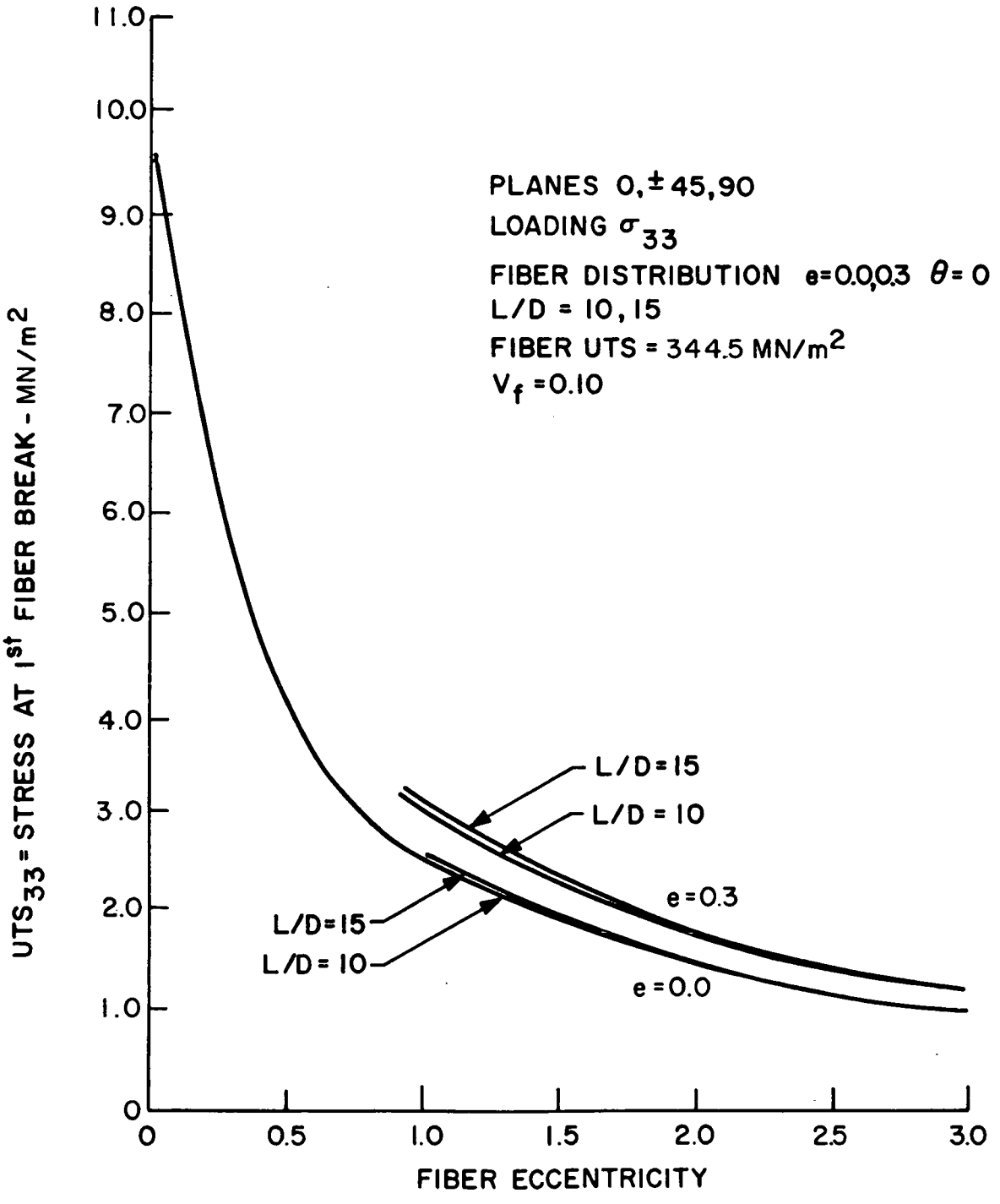

Figure 27 - Effect of fiber eccentricity on strength.

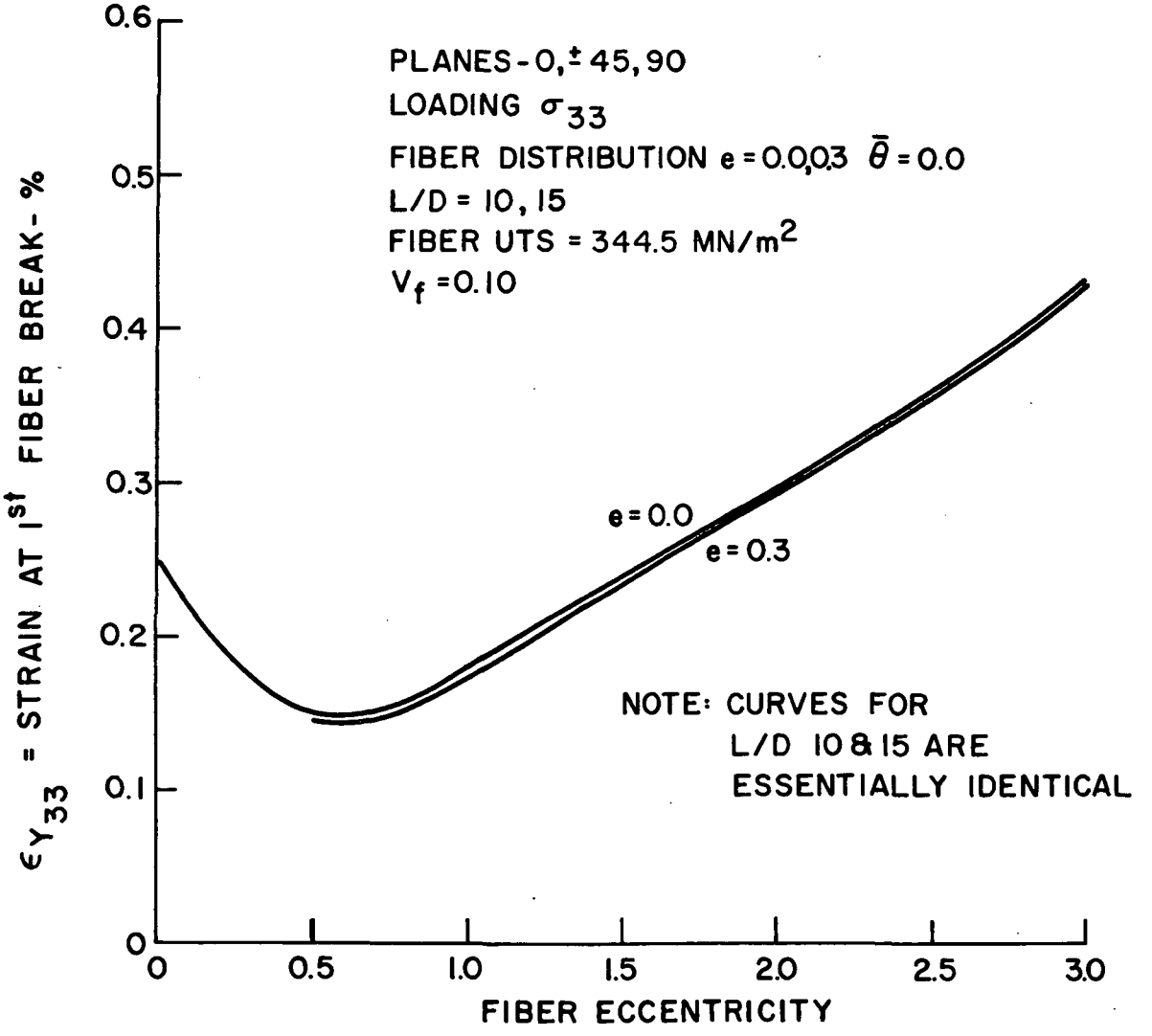

Figure 28 - Effect of fiber eccentricity on strain at first fiber break.

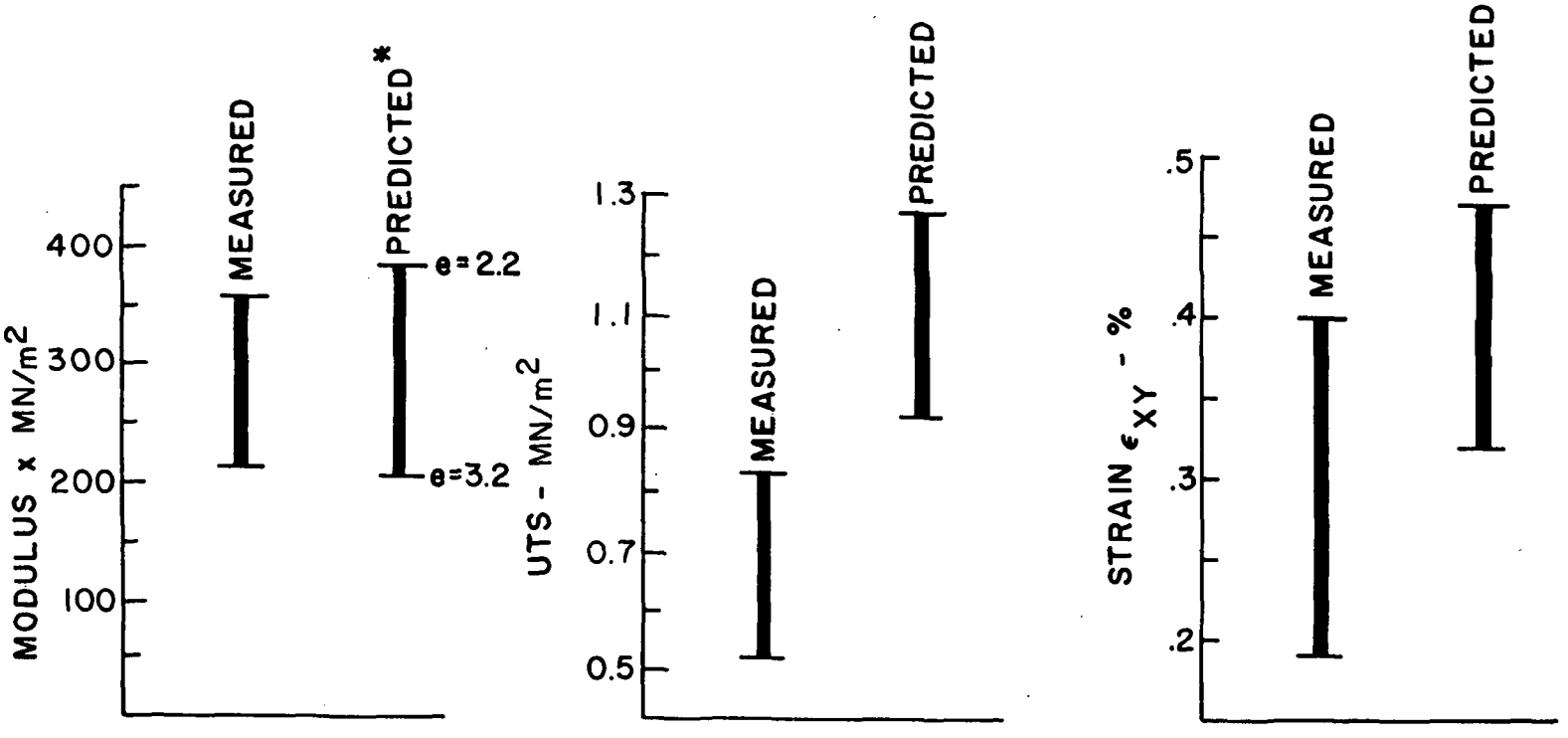

* PREDICTED VALUES FROM FIG. 26,27,28 WITH $\epsilon = 0$ AND FIBER ECCENTRICITY FROM 2.2 TO 3.2

Figure 29 - Comparison between predicted and measured properties for MOD 1B

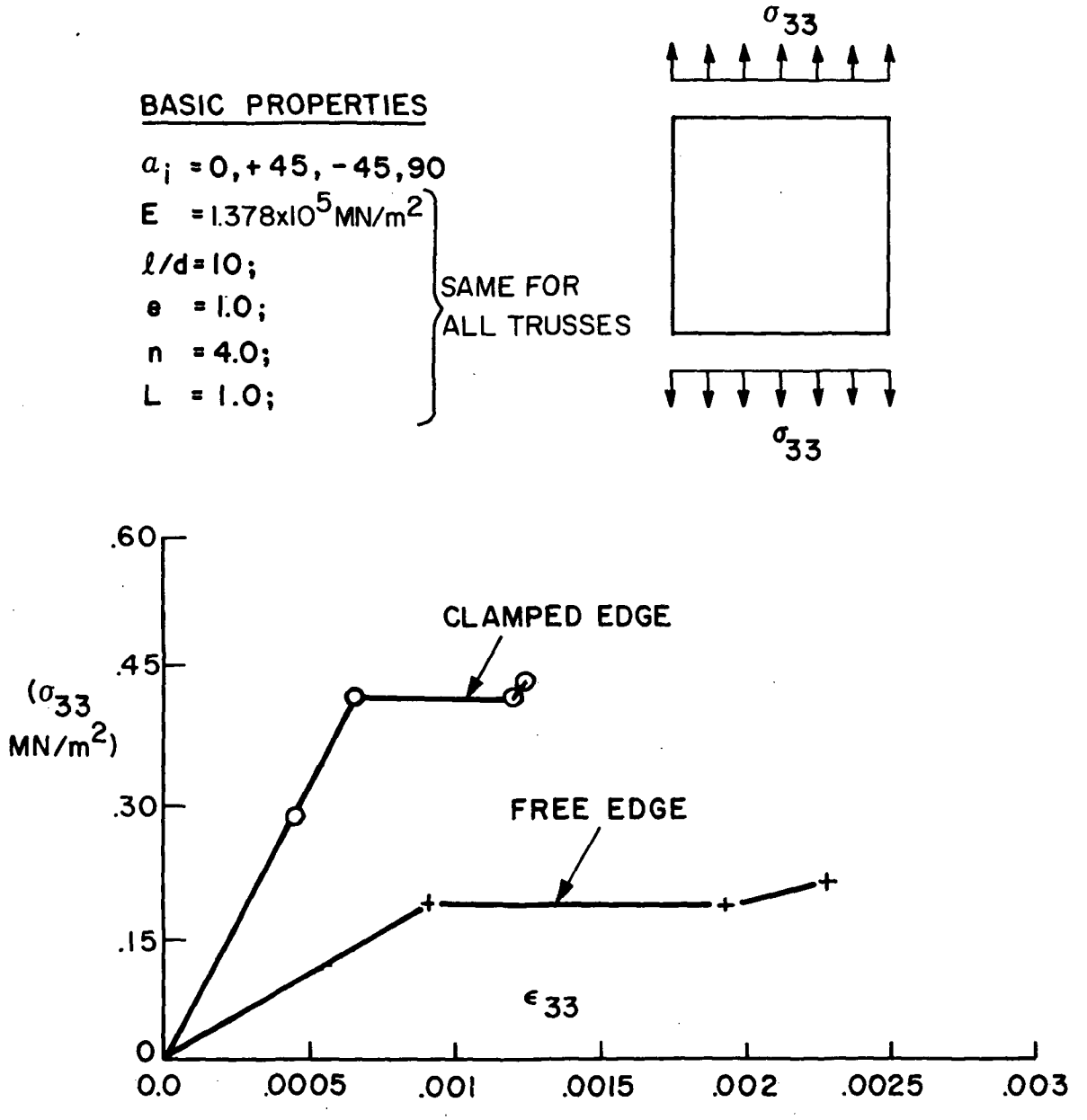

Figure B-1a - Stress-strain behavior of RSI material considering strength variability (volume fraction = 5%).

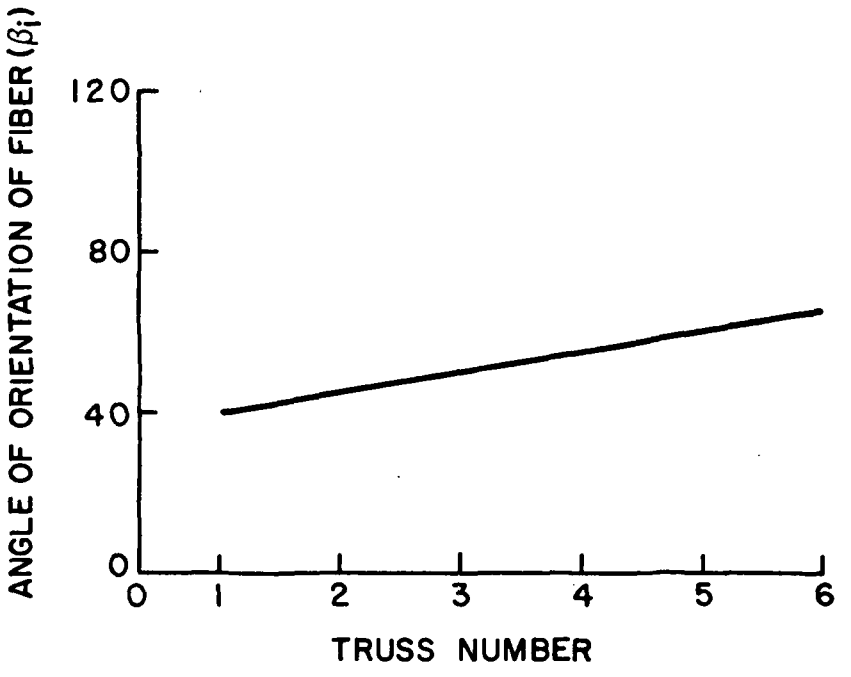

Figure B-1b - Angle of orientation of fiber in any plane.

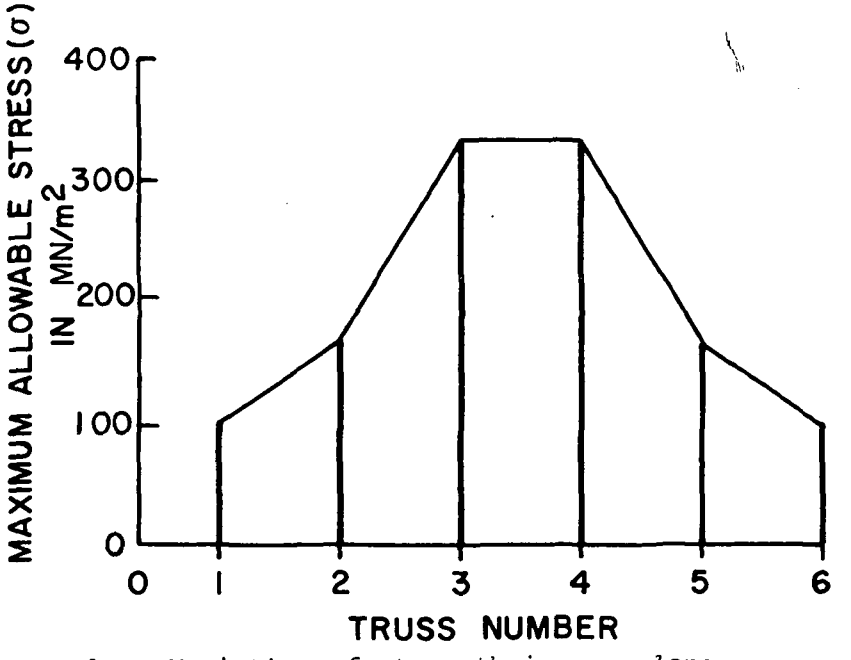

Figure B-1c - Variation of strength in any plane.

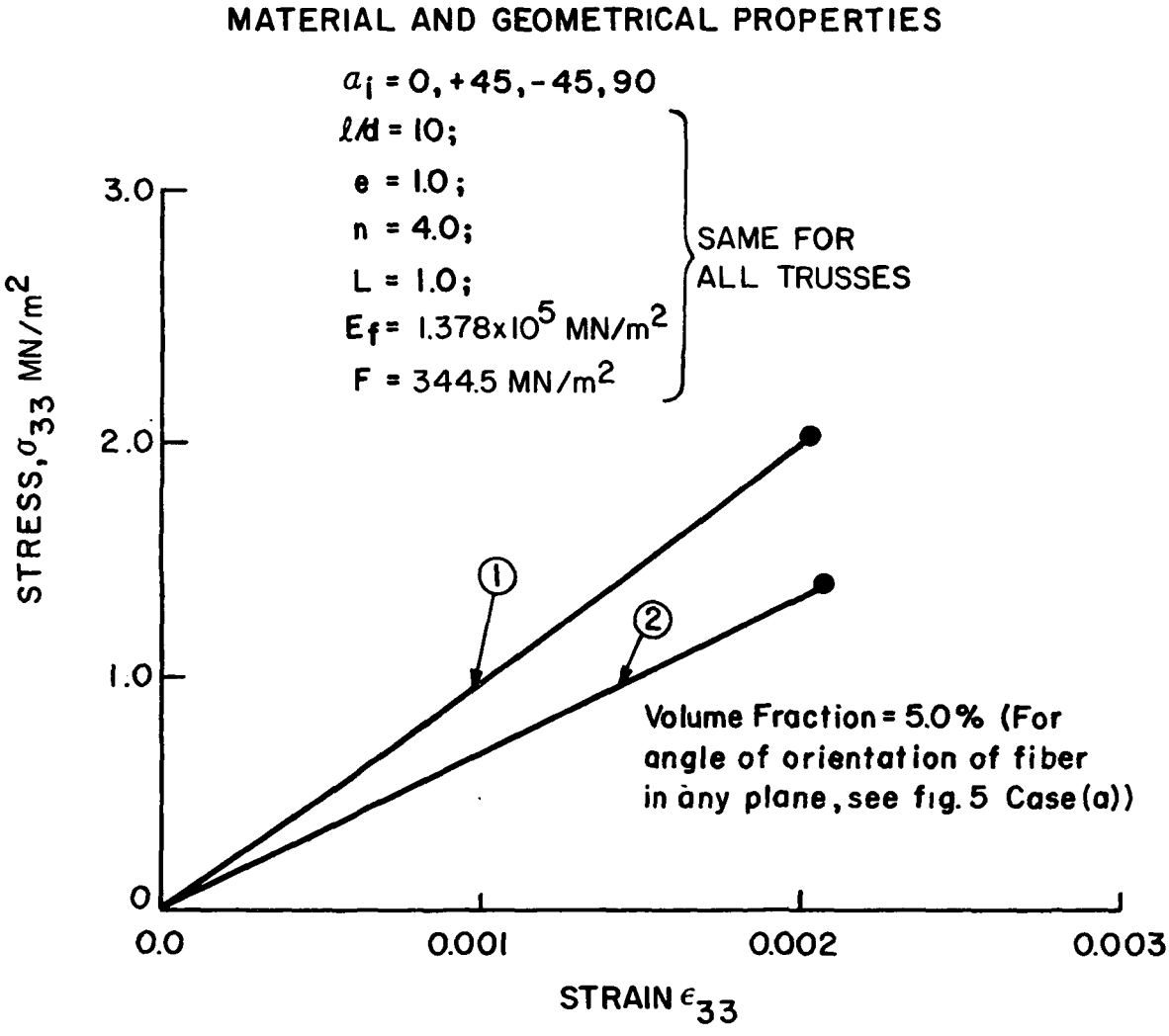

Figure B-2 - Stress-strain behavior of RSI model under tension.

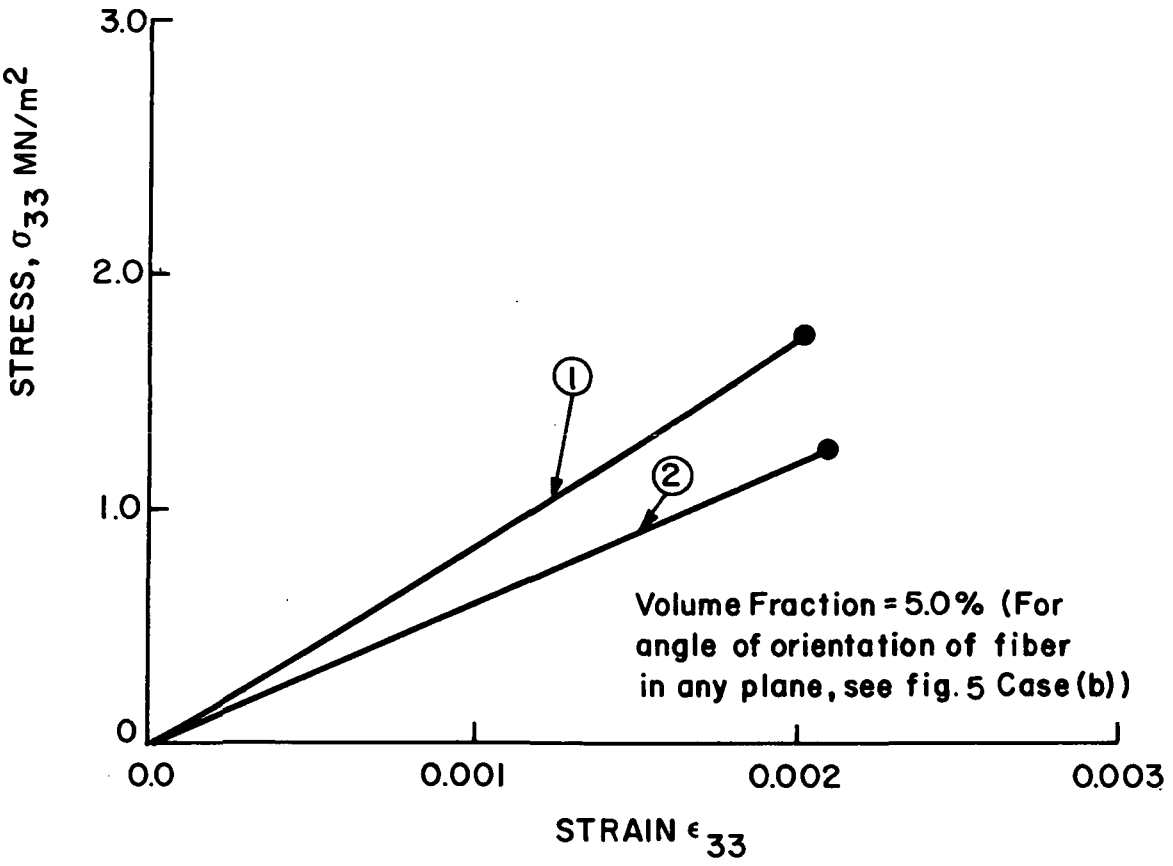

Figure B-3 - Stress-strain behavior of RSI model under tension.

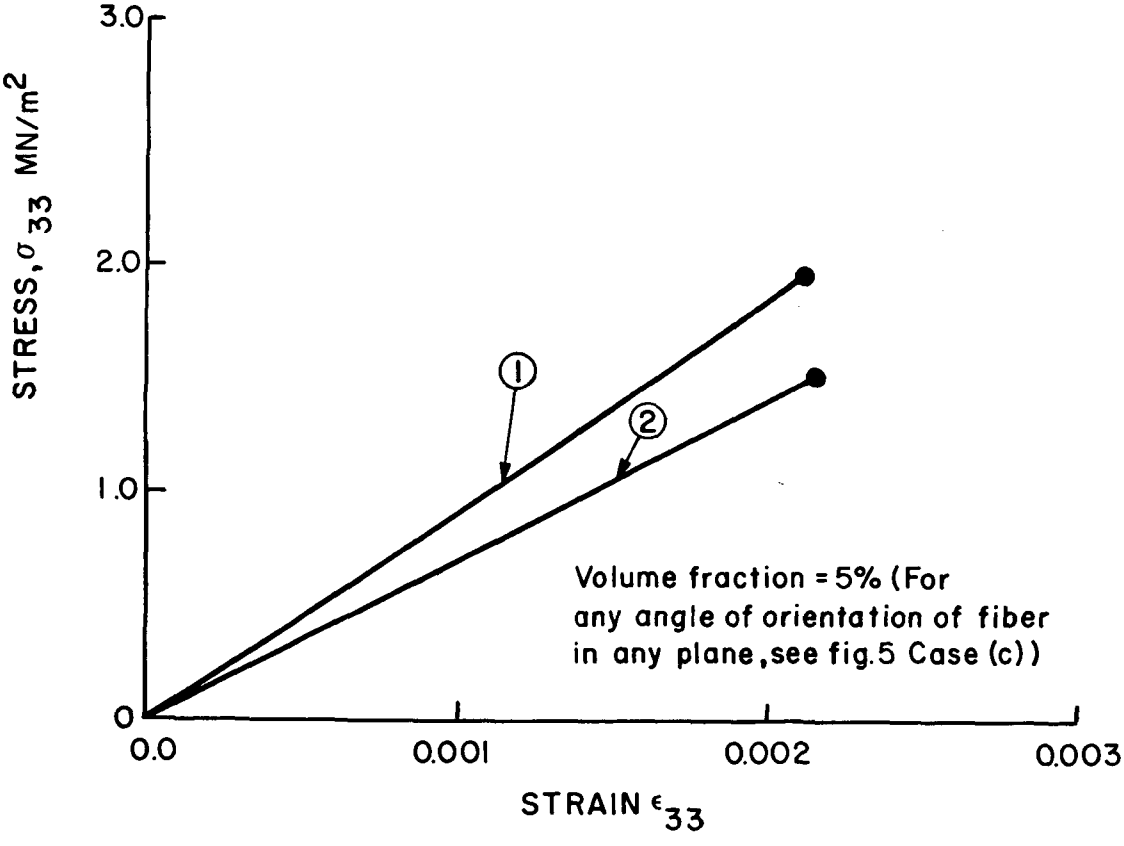

Figure B-4 - Stress-strain behavior of RST model under tension.

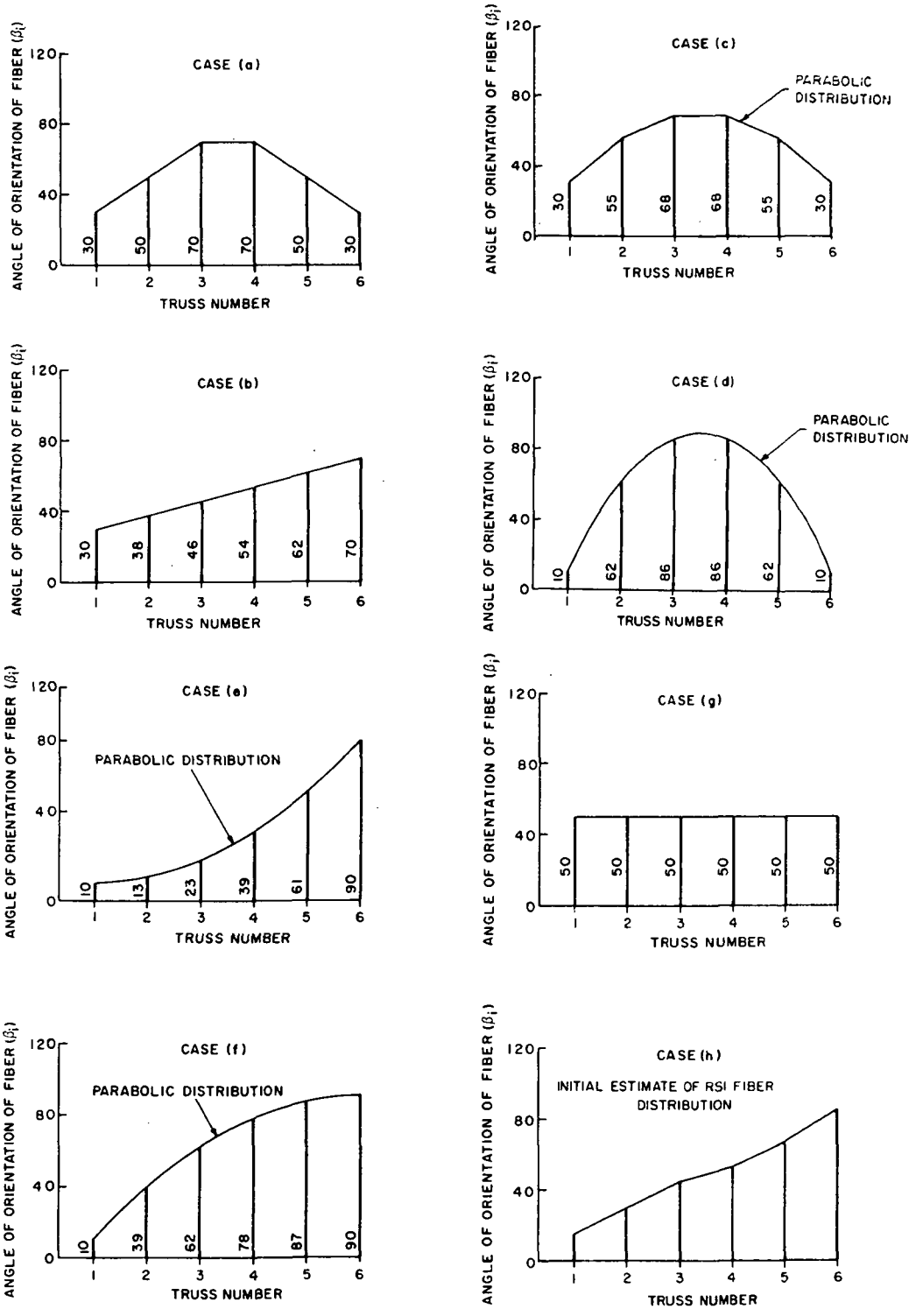

Figure B-5 - Variability of angle of orientation of the fiber different trusses in any plane.

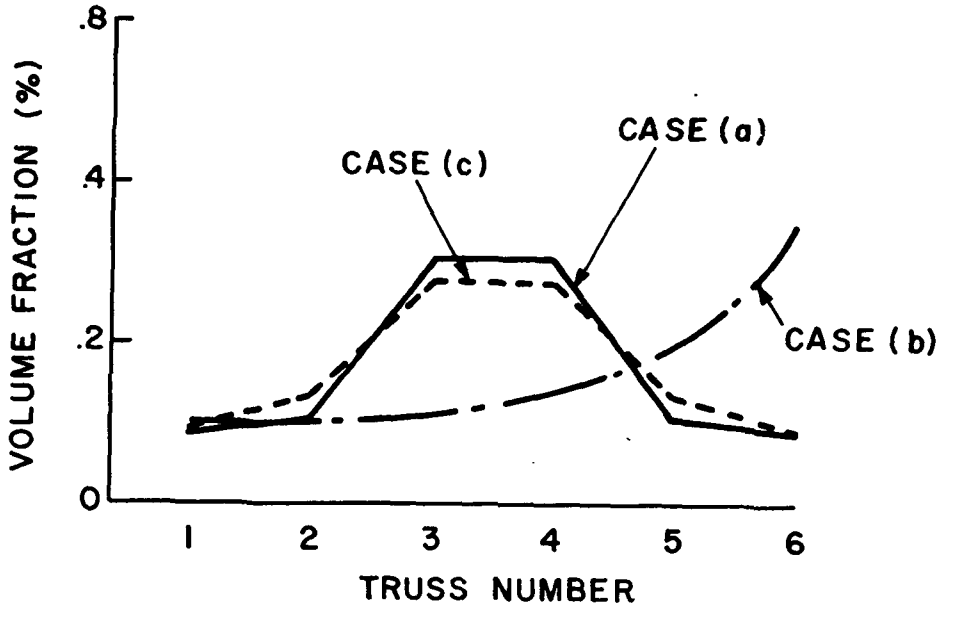

Figure B-6 - Variability of volume fraction of different trusses in a plane.

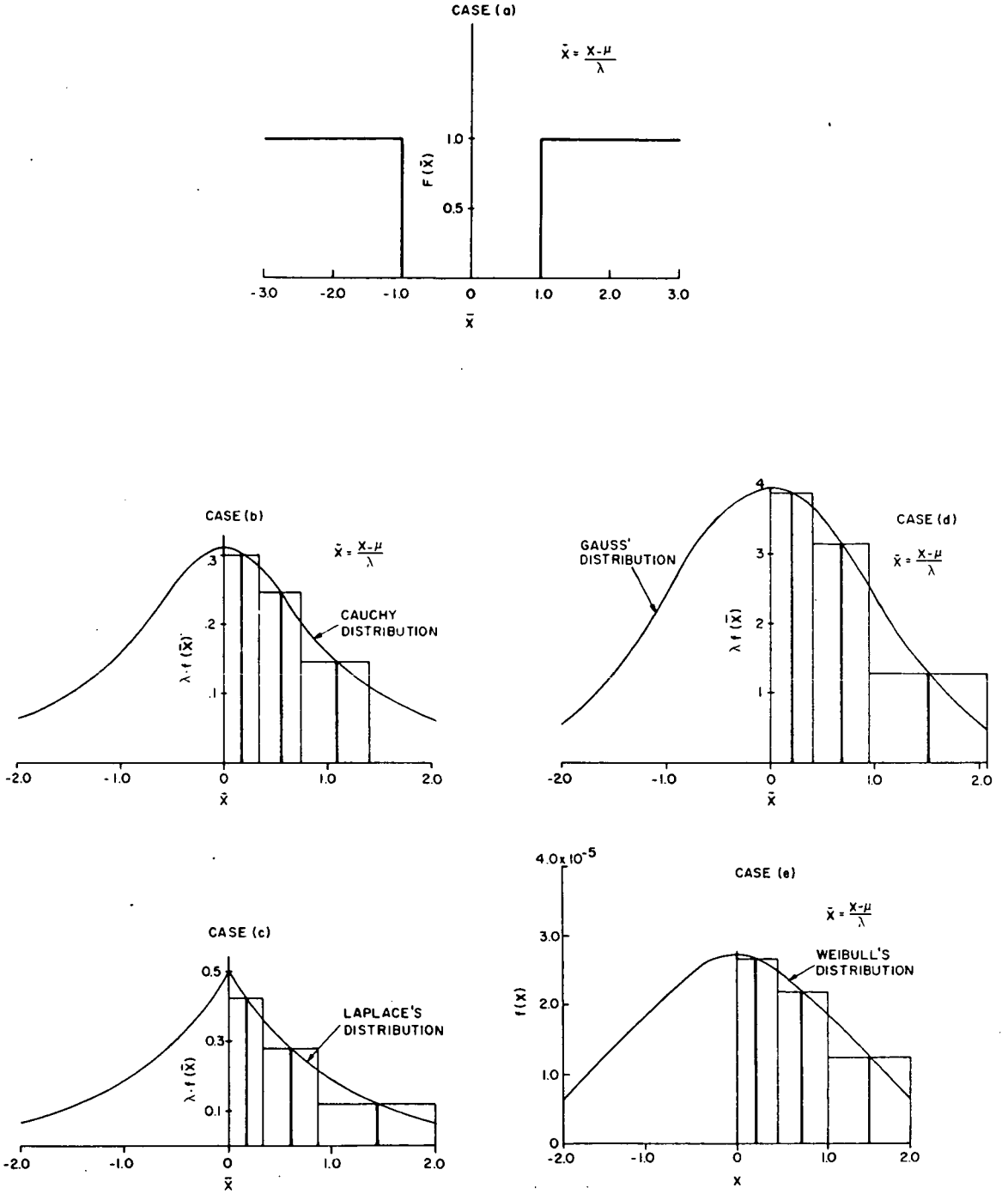

Figure B-7 - Variability of strength distribution of fibers in trusses in any plane.

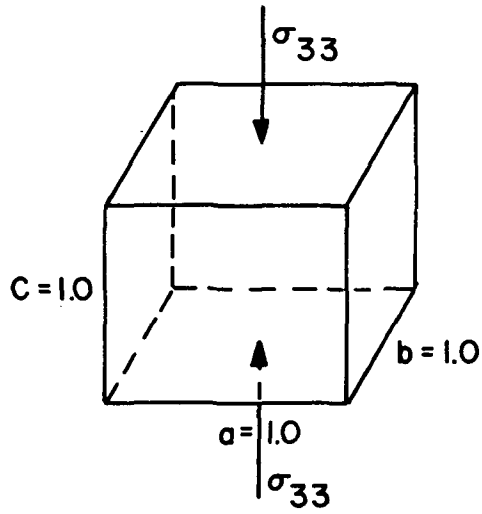

MATERIAL AND GEOMETRICAL PROPERTIES:

L/D = 10;
e = 1.0;
n = 4.0;
L = 1.0;
E_f = 1.378×10^5 MN/m^2
F = 344.5 MN/m^2

} SAME FOR ALL TRUSSES

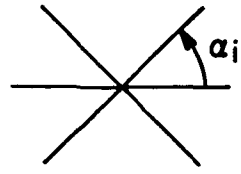

α_i = 0, +45, -45, 90

LAYOUT OF VERTICAL TRUSS.
SIX TRUSSES IN EACH PLANE

Figure B-8 - RSI model used for compression, shear and combined tension/shear loading.

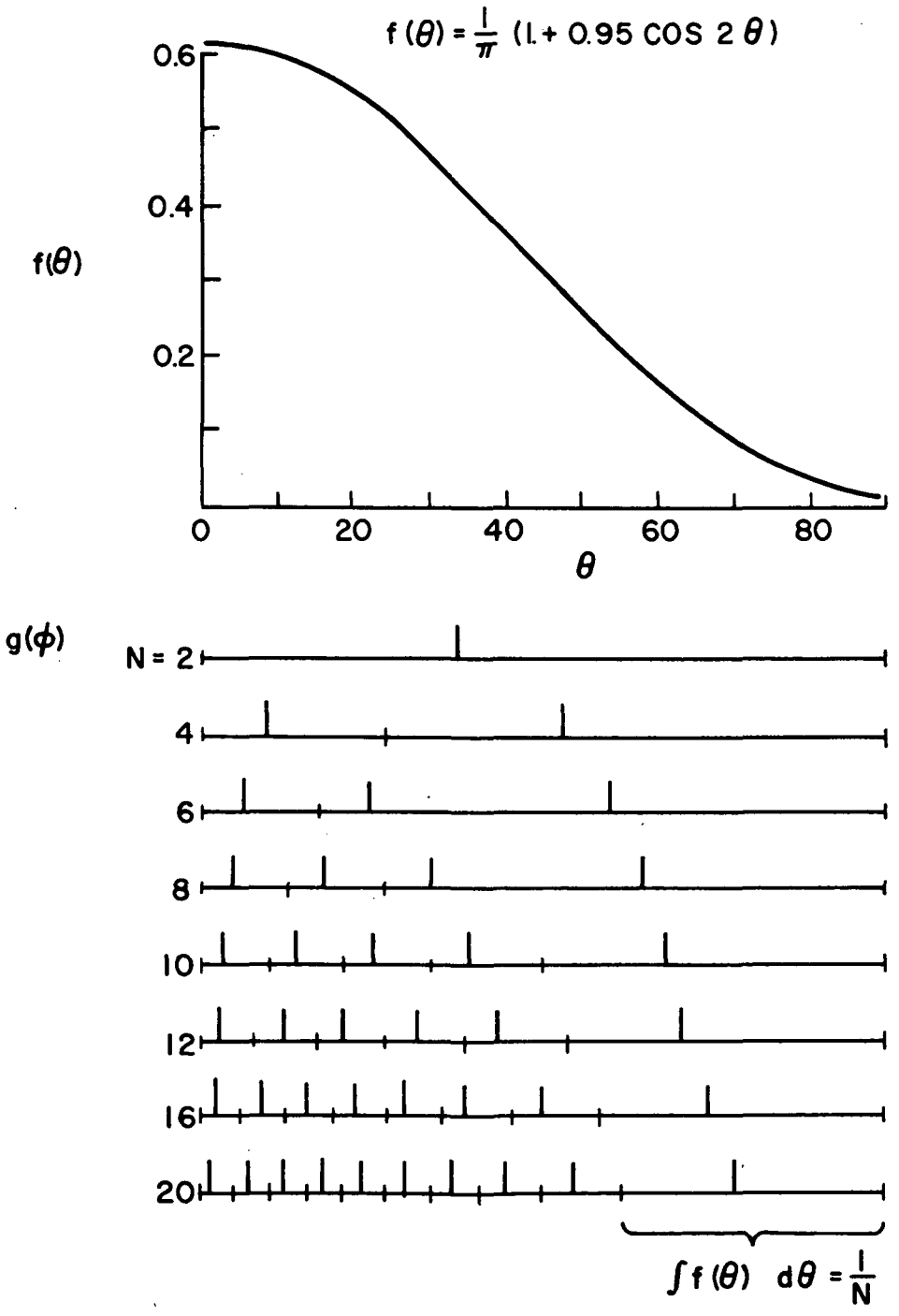

Figure C-1 - Continuous and discrete distributions

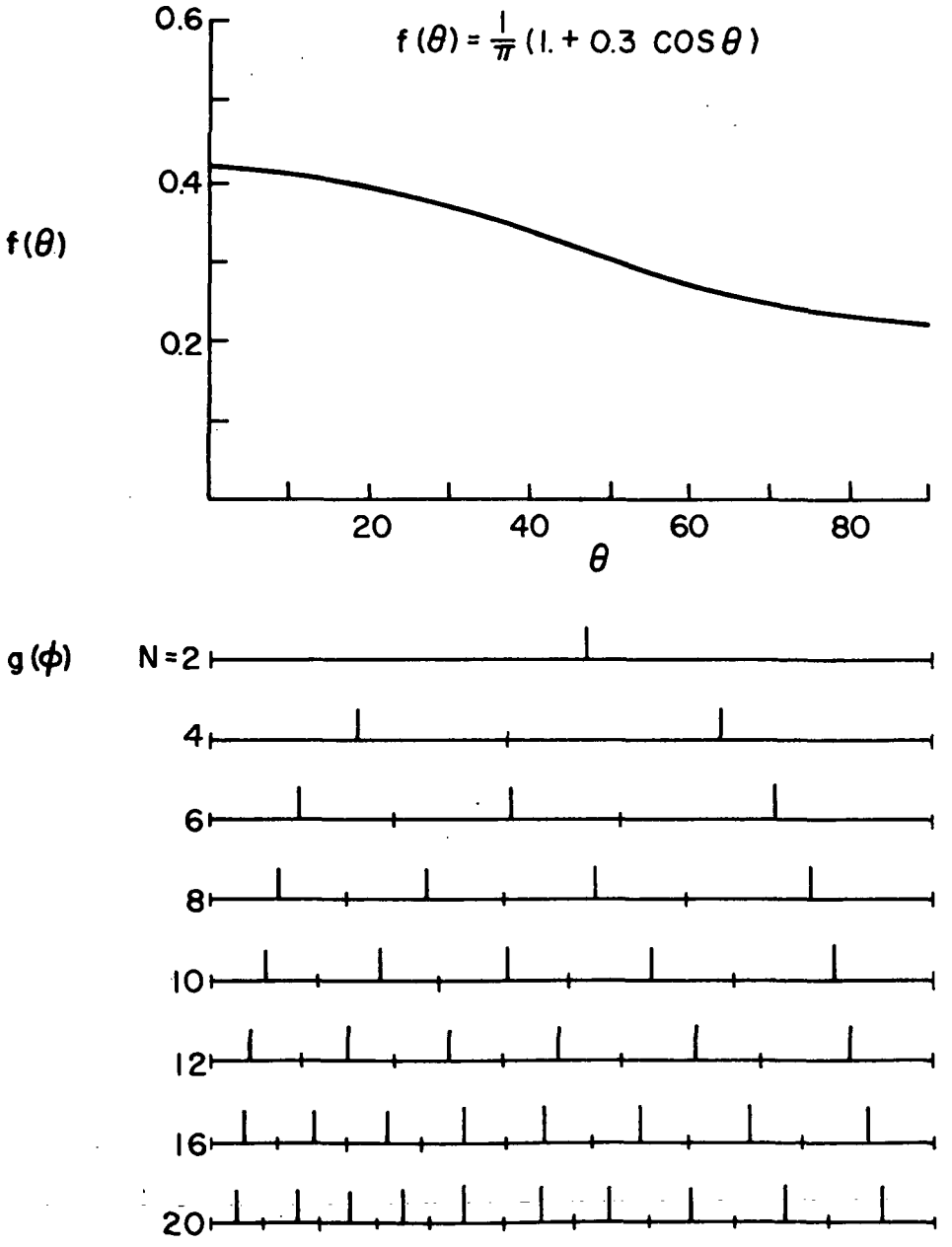

Figure C-2 - Continuous and discrete distributions

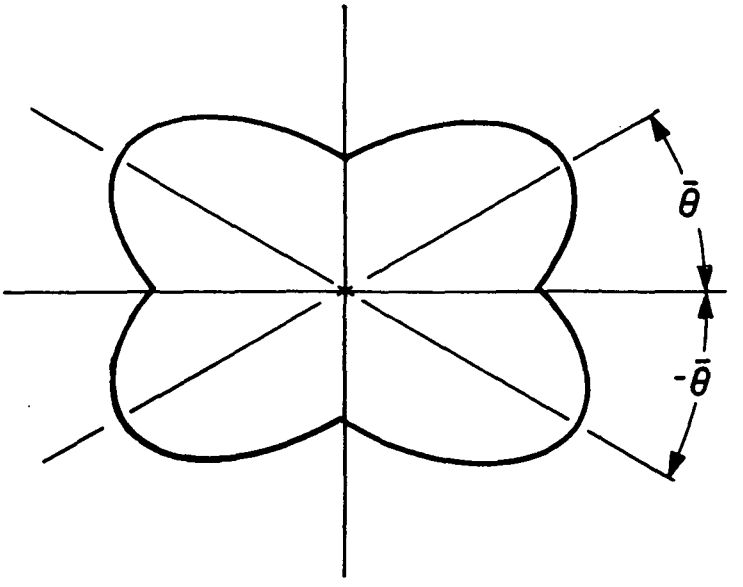

$$f(\theta) = \frac{1 + e \cos 2(\theta - j\bar{\theta})}{\pi + 2e \sin 2\bar{\theta}}$$

$j = +1$ if $0 \leq \theta \leq \pi/2$

$\pi < \theta \leq 3\pi/2$

$j = -1$ if $\pi/2 < \theta \leq \pi$

$3\frac{\pi}{2} < \theta < 2\pi$

Figure C-3 - Fiber distribution for RSI material

NATIONAL AERONAUTICS AND SPACE ADMINISTRATION
WASHINGTON, D.C. 20546

OFFICIAL BUSINESS
PENALTY FOR PRIVATE USE $300

SPECIAL FOURTH-CLASS RATE BOOK

POSTAGE AND FEES PAID
NATIONAL AERONAUTICS AND SPACE ADMINISTRATION
451

U.S.MAIL

POSTMASTER: If Undeliverable (Section 158 Postal Manual) Do Not Return

"The aeronautical and space activities of the United States shall be conducted so as to contribute . . . to the expansion of human knowledge of phenomena in the atmosphere and space. The Administration shall provide for the widest practicable and appropriate dissemination of information concerning its activities and the results thereof."

—NATIONAL AERONAUTICS AND SPACE ACT OF 1958

NASA SCIENTIFIC AND TECHNICAL PUBLICATIONS

TECHNICAL REPORTS: Scientific and technical information considered important, complete, and a lasting contribution to existing knowledge.

TECHNICAL NOTES: Information less broad in scope but nevertheless of importance as a contribution to existing knowledge.

TECHNICAL MEMORANDUMS: Information receiving limited distribution because of preliminary data, security classification, or other reasons. Also includes conference proceedings with either limited or unlimited distribution.

CONTRACTOR REPORTS: Scientific and technical information generated under a NASA contract or grant and considered an important contribution to existing knowledge.

TECHNICAL TRANSLATIONS: Information published in a foreign language considered to merit NASA distribution in English.

SPECIAL PUBLICATIONS: Information derived from or of value to NASA activities. Publications include final reports of major projects, monographs, data compilations, handbooks, sourcebooks, and special bibliographies.

TECHNOLOGY UTILIZATION PUBLICATIONS: Information on technology used by NASA that may be of particular interest in commercial and other non-aerospace applications. Publications include Tech Briefs, Technology Utilization Reports and Technology Surveys.

Details on the availability of these publications may be obtained from:

SCIENTIFIC AND TECHNICAL INFORMATION OFFICE

NATIONAL AERONAUTICS AND SPACE ADMINISTRATION

Washington, D.C. 20546